AAS 99-073

TRMM On-Orbit Attitude Control System Performance

Brent Robertson, Sam Placanica, Wendy Morgenstern

NASA Goddard Space Flight Center

22nd ANNUAL AAS GUIDANCE AND CONTROL CONFERENCE

February 3-7, 1999
Breckenridge, Colorado

Sponsored by
Rocky Mountain Section

AAS Publications Office, P.O. Box 28130 - San Diego, California 92198

AAS-99-073

TRMM ON-ORBIT ATTITUDE CONTROL SYSTEM PERFORMANCE

Brent Robertson*, Sam Placanica**, Wendy Morgenstern**
NASA Goddard Space Flight Center

This paper presents an overview of the Tropical Rainfall Measuring Mission (TRMM) Attitude Control System (ACS) along with detailed in-flight performance results for each operational mode. TRMM is a joint mission between NASA and the National Space Development Agency (NASDA) of Japan designed to monitor and study tropical rainfall and the associated release of energy. The TRMM spacecraft is an Earth-pointed, zero momentum bias satellite launched on November 27, 1997 from Tanegashima Space Center, Japan. Launched to provide a validation for poorly known rainfall data sets generated by global climate models, TRMM has demonstrated its utility by reducing uncertainties in global rainfall measurements by a factor of two.

The ACS is comprised of Attitude Control Electronics (ACE), an Earth Sensor Assembly (ESA), Digital Sun Sensors (DSS), Inertial Reference Units (IRU), Three Axis Magnetometers (TAM), Coarse Sun Sensors (CSS), Magnetic Torquer Bars (MTB), Reaction Wheel Assemblies (RWA), Engine Valve Drivers (EVD) and thrusters. While in Mission Mode, the ESA provides roll and pitch axis attitude error measurements and the DSS provide yaw updates twice per orbit. In addition, the TAM in combination with the IRU and DSS can be used to provide pointing in a contingency attitude determination mode which does not rely on the ESA. Although the ACS performance to date has been highly successful, lessons were learned during checkout and initial on-orbit operation. This paper describes the design, on-orbit checkout, performance and lessons learned for the TRMM ACS.

TRMM MISSION OVERVIEW

TRMM is a joint mission between NASA and the National Space Development Agency (NASDA) of Japan designed to monitor and study tropical rainfall and the associated release of energy shaping both weather and climate around the globe. TRMM is the first mission dedicated to measuring rainfall through five microwave and visible infrared sensors, including the first spaceborne rain radar. Launched to provide a validation for poorly known rainfall data sets generated by global climate models, TRMM has demonstrated its utility by reducing uncertainties in global rainfall measurements by a factor of two. A sample image taken by one of the TRMM instruments is shown in Figure 1.

* Branch Head, Guidance, Navigation & Control System Engineering, Phone: (301) 286-6392, email: brent.robertson@gsfc.nasa.gov
** Aerospace Engineer, Flight Dynamics & Analysis Branch

TRMM Microwave Imager Data (TMI)

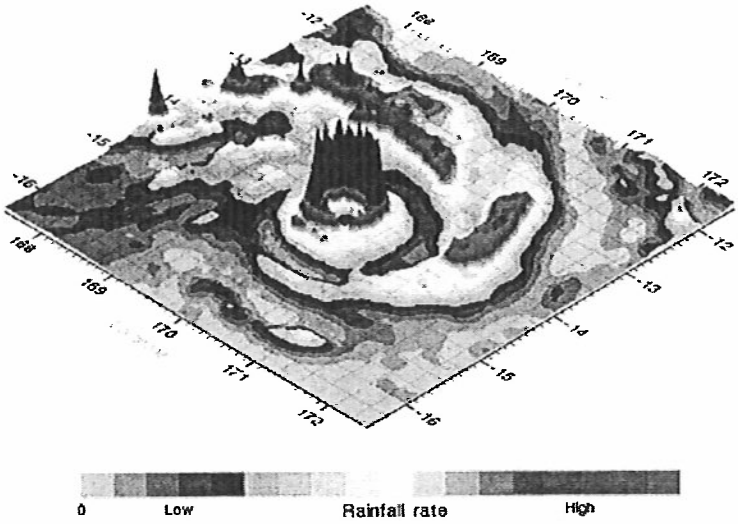

Cyclone Susan, 5th January 1998

980107 C.Kidd

Figure 1 TRMM Science Image

The TRMM spacecraft, shown in Figure 2, was launched on the H-II Expendable Launch Vehicle on November 27, 1997 from Tanegashima Space Center, Japan. The spacecraft is three-axis stabilized, in a near circular 350 km orbit with inclination of 35^{o}. At launch, the spacecraft had a mass of 3,523 kg including 903 kg of fuel and pressurant. Solar arrays are canted at a 26.5 angle from the YZ plane and track about the Y-axis via a Solar Array Drive Assembly (SADA).

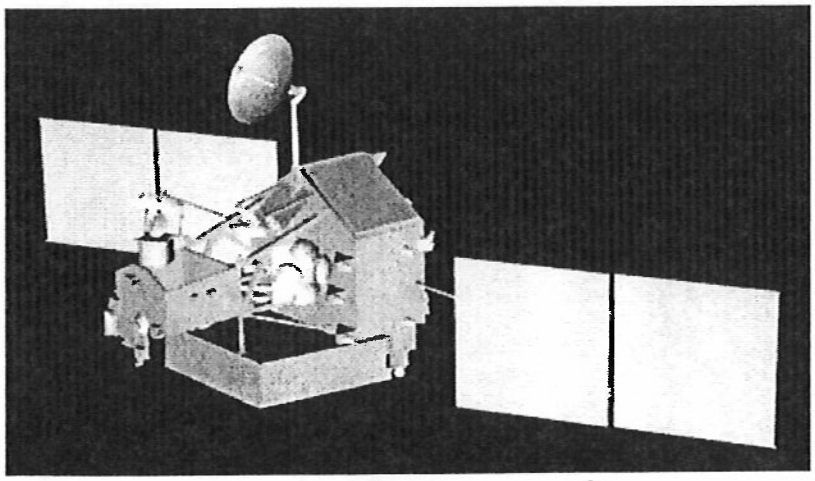

Figure 2 TRMM Spacecraft

TRMM ATTITUDE CONTROL SYSTEM DESIGN

The TRMM Attitude Control System (ACS) is required to maintain a nadir pointing attitude with requirements shown in Table 1[1]. Since the science requirement did not specify either a geocentric or geodetic reference, for convenience the nadir reference was defined by the output of the chosen Earth sensor. This resulted in a nadir reference defined by a horizon bisector of the CO_2 horizon of the Earth, so that spacecraft pointing is provided with respect to a quasi-geodetic position. Analysis shows that this reference is approximately 0.01^0 from the geodetic frame with nominal ESA performance. The ACS is required to provide the ability to acquire Mission Mode given worse case H-II tip-off rates and any spacecraft attitude.

Table 1
TRMM ACS MISSION MODE POINTING REQUIREMENTS

Characteristic	Requirement (per axis)
Pointing Knowledge, on-board (3σ)	0.2^O
Pointing Accuracy (3σ)	0.4^O
Stability (peak to peak)	0.1^O over 1 sec

Due to an instrument thermal requirement that the +Y side of the spacecraft stay cold, the Mission Mode is required to operate in either a +X forward or –X forward orientation. The spacecraft is required to rotate 180^0 about nadir (yaw) every few weeks when the Sun crosses the orbit plane. Due to these yaw rotations, the spacecraft maintains an angle between the Sun and the spacecraft X-Z plane of roughly between 0^0 and 58.4^0.

The TRMM mission requires an orbit of 350 km altitude with tolerance of +/- 1.25 km. The ACS is required to provide thruster-based control modes to maintain the orbit and provide backup momentum unloading and slew capabilities. The ACS is also required to provide solar array tracking and High Gain Antenna (HGA) pointing throughout the mission.

The TRMM ACS architecture is shown in Figure 3. The ACS is comprised of Attitude Control Electronics (ACE), an Earth Sensor Assemble (ESA), Digital Sun Sensors (DSS), Inertial Reference Units (IRU), Three Axis Magnetometers (TAM), Coarse Sun Sensors (CSS), Magnetic Torquer Bars (MTB), Reaction Wheel Assemblies (RWA), Engine Valve Driver (EVD) and thrusters. Each EVD can drive up to 12 hydrazine thrusters. The ACE is comprised of an 80C86 processor, DC-DC converters, and actuator and sensor interface electronics. The ACE processor formats raw sensor data, decodes commands and contains Safe Hold flight software. The ACE transmits the sensor data over a 1773 fiber optics data bus to a 80386 processor, referred to as the ACS processor, to be used by the ACS software and down-linked in telemetry. The flight software for initialization, attitude determination and control, momentum management, ephemeris generation, solar array commanding, High Gain Antenna (HGA) commanding,

mode management and Fault Detection and Correction (FDC) are implemented in the ACS Processor. The FDC software provides tolerance of a single point failure with minimal interruption to science data gathering. The computed control torques are sent back to the ACE, which relays the appropriate commands to the actuators. The TRMM ACS operates at a 2 Hz control rate while in all modes with the exception of the thruster-based modes which operate at 8 Hz. All TRMM ACS components are fully redundant and cross-strapped with the exception of the MTBs which have redundant windings that are not cross-strapped.

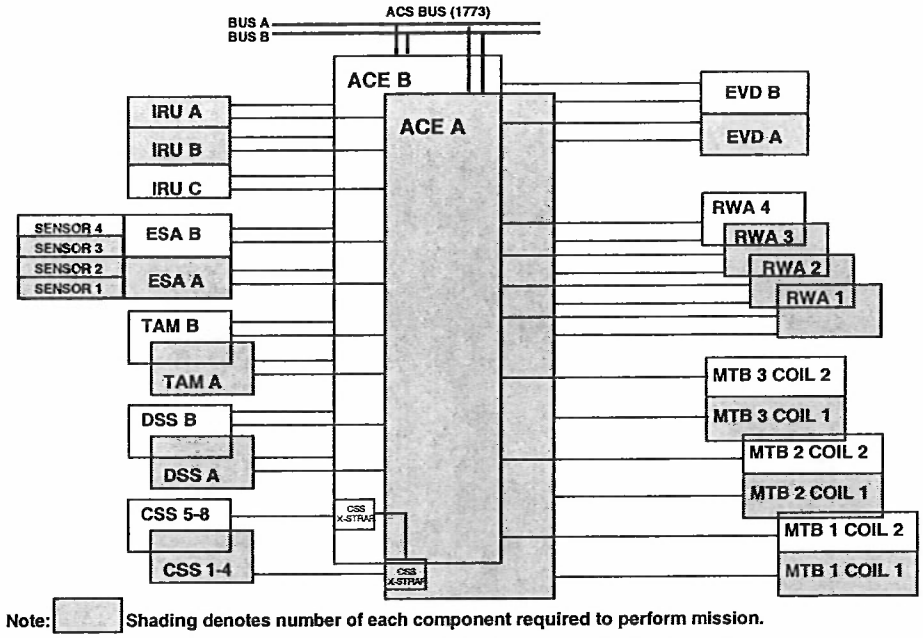

Figure 3 TRMM ACS Architecture

Table 2 shows the various ACS modes of operation, associated equipment used, and function of each mode. While in Mission Mode, the ESA provides roll (X) and pitch (Y) axis attitude error measurements. Yaw (Z) position is determined with DSS updates and propagated between updates using gyro output. Four RWAs arranged in a pyramid configuration are used for control. The TAM and three MTBs are used for momentum management.

Table 2
TRMM ACS MODES

Mode	Equipment Used	Function
Standby	80386, ACE CSS, IRU, TAM	ACS Mode entered during launch or while ACE in Safe Hold.
Sun Acquisition	80386, ACE CSS, IRU, TAM RWA, MTB	Acquire Sun-pointing attitude. Solar arrays commanded to index position.
Earth Acquisition	80386, ACE ESA, IRU, TAM RWA, MTB	Point +Z axis to nadir.
Yaw Acquisition	80386, ACE ESA, IRU, TAM RWA, MTB	Align +X or –X axis with velocity vector. Solar arrays commanded to track Sun when yaw attitude is within 10^0.
Mission	80386, ACE ESA, DSS, IRU, TAM RWA, MTB	Provide nadir pointing orientation for Science operation. Solar arrays track Sun. Orientation Sub-modes: +X forward, -X forward, -Y forward, Yaw Maneuver Attitude Determination Sub-modes: Normal, Contingency (does not use ESA)
CERES Calibration	80386, ACE IRU, TAM RWA, MTB	Maintain spacecraft inertially fixed for CERES instrument calibration.
Delta V	80386, ACE IRU EVD, Thrusters	Control spacecraft attitude during orbit adjust maneuvers. Sub-modes: +X forward, -X forward
Delta H	80386, ACE IRU EVD, Thrusters	Control spacecraft momentum. Backup yaw maneuver.
Safe Hold	ACE CSS, IRU, TAM RWA, MTB	ACE mode to acquire Sun-pointing attitude. Solar arrays commanded to index position. ACS resides in Standby.

The initial mode entered upon separation from the launch vehicle is the wheel-based Sun Acquisition Mode. In this mode, solar arrays are commanded to an indexed position (solar array normal toward +X axis) and the spacecraft acquires a Sun-pointing attitude. Sun Acquisition Mode uses the full capability of both MTBs to increase momentum unloading capability over Mission Mode. If spacecraft momentum is above a set limit when entering Sun Acquisition, RWA control to the Sun is not attempted while the MTBs unload momentum in order to conserve power. Once a valid ephemeris has been loaded in Sun Acquisition Mode, the spacecraft may be commanded to Earth Acquisition Mode at any point in the orbit. Transition through Yaw Acquisition Mode to Mission Mode is autonomous.

Mission Mode is a wheel-based mode where all instrument science is performed. This mode allows the +X, -X or -Y spacecraft axis to be flown along the velocity vector. The –Y orientation is used occasionally throughout the mission for the instrument Precipitation Radar (PR) pattern mapping. Roll and pitch attitude is nominally computed

by the ESA. Yaw attitude is propagated over the orbit by the IRU and updated twice per orbit by each DSS. A contingency attitude determination algorithm using a Kalman filter with DSS, TAM and IRU data (no ESA) can also provide slightly degraded pointing from the 0.2^0 knowledge requirement. This mode was provided due to concerns that the ESA may have a single point failure. Yaw maneuvers to and from the +X, -X or –Y orientations are accomplished while in Mission Mode. Solar arrays are commanded to track the Sun while in the daylight. During eclipse, the solar arrays are commanded to an edge-on "feathered" position in order to reduce aerodynamic drag.

Delta V Mode is commanded for all orbit adjust maneuvers. Orbit adjust maneuvers are required for mission orbit acquisition (descent from 380 km to 350 km), orbit maintenance and controlled reentry. This mode autonomously transfers through Earth Acquisition and Yaw Acquisition to Mission Mode once the burn has been completed. A Delta V may be performed in either the +X or -X direction. Four thrusters are located on the Instrument Support Platform (ISP) with thrust directions nominally along the +X axis and four other thrusters are located on the Lower Bus Structure (LBS) with thrust directions nominally along the –X axis. Either the ISP or LBS thrusters provide pitch and yaw control during the burn through off-modulation. Roll control during the burn is provided by on-modulation of four additional roll control thrusters with thrust directions radial to the X-axis.

CERES Calibration Mode is an inertial-fixed, wheel–based mode designed to be entered at orbit noon for one orbit. This mode provides calibration of the CERES instrument. CERES Calibration Mode is exited by command to Earth Acquisition Mode.

Delta H Mode is the only mode on TRMM that has not been entered to date. This mode allows the spacecraft to unload a set amount of momentum and can be used as a backup to momentum unloading with magnetics at low altitudes during controlled re-entry. The Delta H Mode also provides backup yaw slews.

All ACS modes autonomously transfer to Standby Mode if the ACE enters Safe Hold Mode. Safe Hold Mode is functionally equivalent to Sun Acquisition Mode, but utilizes independent software coded in a different software language. Safe Hold Mode resides in the ACE processor, which provides hardware independence from the ACS processors. Safe Hold Mode was designed to be wheel based to avoid large changes in spacecraft momentum state which can result from the misuse of thrusters. While in Standby Mode, three-axis attitude is provided by the ACS processor through a TRIAD algorithm using TAM, DSS and IRU data. The performance of the Sun Acquisition Mode can also be monitored while the ACE is in Safe Hold Mode. Figure 4 illustrates valid mode transitions.

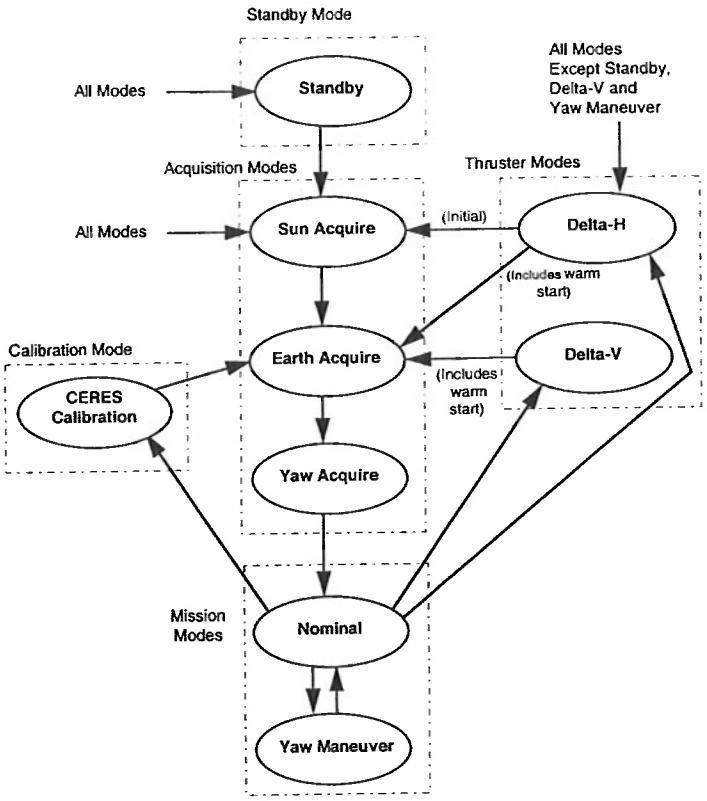

Figure 4 TRMM ACS Mode Transitions

LAUNCH AND ON-ORBIT CHECKOUT

Launch and initial operation of the TRMM ACS was very smooth. Upon separation from the H-II and deployment of the TRMM solar arrays and HGA, the RWAs were autonomously powered by the spacecraft sequencer and the spacecraft transitioned from Standby Mode to Sun Acquisition Mode. The H-II tip-off rates, as monitored by the IRU, were -0.02, -0.13 and 0.04 degrees/second for roll, pitch and yaw, respectively. These were well below even the 1-σ tip-off rates specified for the H-II. Due to the low spacecraft system momentum, four RWAs were immediately used to acquire the Sun in less than 10 minutes. Figure 5 shows gyro rates during the launch and acquisition. Figure 6 illustrates position errors while in Sun Acquisition Mode.

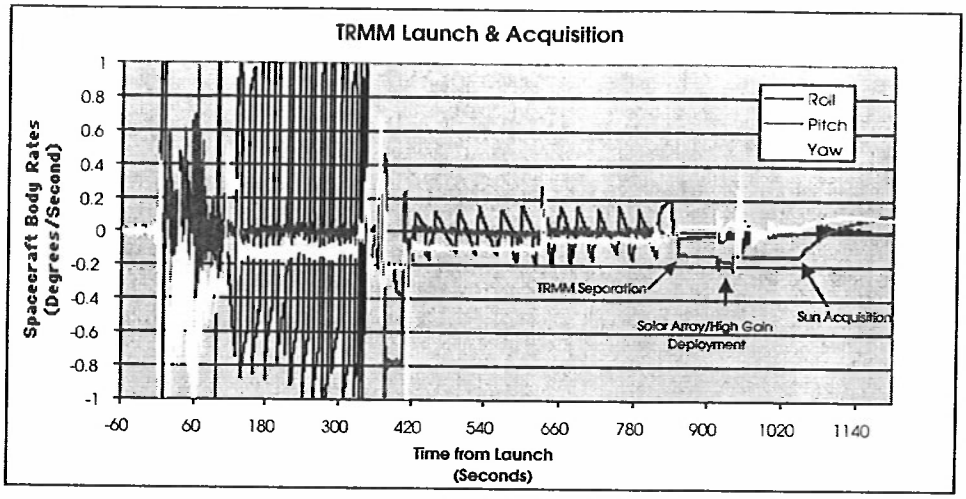

Figure 5 Launch and Acquisition: Gyro Rate

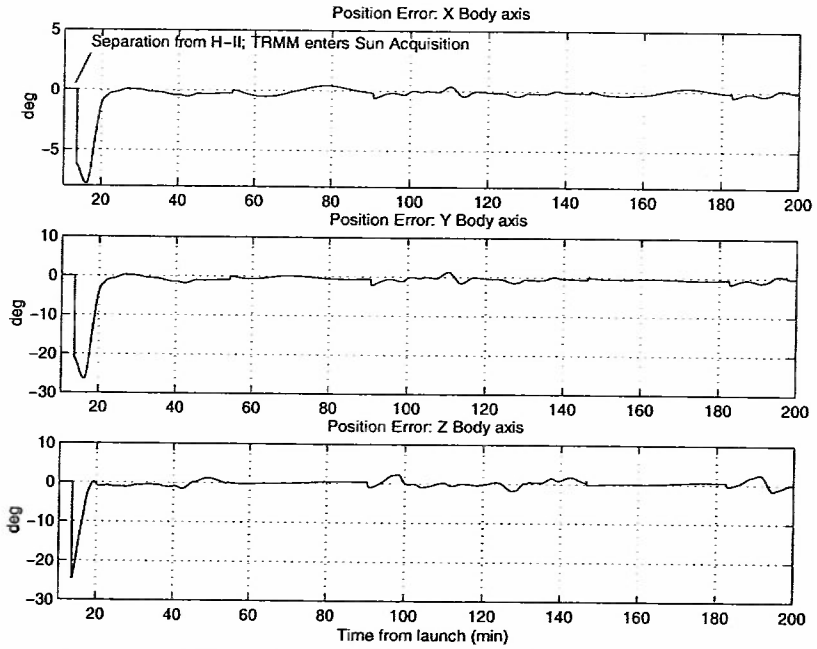

Figure 6 Sun Acquisition Mode: Position Errors

The only ACS anomaly acquisition occurred within the first orbit, when the FDC marked the TAM A as static and autonomously switched to TAM B. This occurred because the on-orbit noise on both TAMs was lower than the static threshold that is used to decide if the TAM data is updating correctly. Although this did not present a problem, because TAM B also had lower noise than expected the next FDC action would have switched control and telemetry from ACE-A to ACE-B. This was avoided to due quick

ground diagnosis and command of the spacecraft to disable the TAM FDC test. The static threshold has since been lowered and TAM A is again being used.

Most of the TRMM ACS subsystem checkout was performed over a five day period during which time the spacecraft was transitioned to Mission Mode. On-orbit checkout consisted of observing system performance during nominal operation and performing three special tests to checkout Safe Hold, Contingency, and thruster modes of operation. Further Contingency Mode testing was done after descent burns were performed to reach the mission altitude of 350 km. Table 3 gives the timeline of events during on-orbit checkout.

Table 3
LAUNCH AND ON-ORBIT CHECKOUT TIMELINE

Time	Event
97-331-21:27:00	Launch
331-21:30:34	Fairing Separation
331-21:41:12	TRMM/H-II Separation
331-21:42:12	Solar Array and HGA pyros fire
331-21:42:42	RWAs powered ON
331-21:42:46	Entered Sun Acquisition Mode
331-21:44:00	+Y Solar Array is indexed
332-01:25	Isolation Valve #5 opened
332-13:17:29	Start of ACS Safe Hold test
332-14:48	End of ACS Safe Hold test
332-15:48	RCS Pyrotechnic Isolation Valve pyro fired, opening valve
332-16:21	Contingency Mode test performed
332-20:30	Exited Contingency Mode. Returned to Sun Acquisition Mode
332-21:03:06	Entered Earth Acquisition Mode
332-21:14:15	ESA Processing transition from Course to Fine
332-21:16:06	Entered Yaw Acquisition Mode
332-21:25:28	Entered Mission Mode
333-14:15:46	Roll thruster 1-shot calibration firings
333-17:58:00	ISP thruster calibration firings
334-15:11:01	10 sec Delta V ISP thruster calibration firing
335-15:03:01	10 sec Delta V LBS thruster calibration firing
337-19:35:01	60 sec Delta V descent burn
338-20:07:01	180 sec Delta V descent burn
339-19:05:01	180 sec Delta V descent burn
339-20:37:01	180 sec Delta V descent burn
340-18:54:01	180 sec Delta V descent burn
340-20:26:01	60 sec Delta V descent burn
341-17:43:38	81 sec Delta V descent burn
341-19:28:42	69.625 sec Delta V descent burn
341-19:29:52	Mission orbit reached
341-20:45:45	Precipitation Radar enters observation mode at mission altitude
346-14:33:00	DSS Alignment Table uploaded
347-13:11:02	First 180° Yaw Maneuver

ACS Safe-Hold Test

One day after launch, TRMM was transitioned from Sun Acquisition to Safe Hold during a planned special test of the Safe Hold operation. This test was performed to ensure that the spacecraft had a safe state to enter should an anomaly occur in the future. The test was done early in the mission to ensure that the mode was fully checked out with engineers familiar with the design who may not be present should the spacecraft transition to Safe Hold in the future.

ACS Contingency Mode Test

While in Sun Acquisition, the ACS Contingency Mode was tested. In Contingency Mode the ACS uses the DSS and TAM data to estimate spacecraft attitude and gyro biases using a Kalman filter algorithm. While in Sun Acquisition Mode the Kalman filter output is available, but it is not used to point the spacecraft. This allowed the performance of the Kalman filter to be tested without affecting spacecraft performance.

Contingency Mode was tested using DSS and TAM data, and during eclipse when only the TAM data was available. When the Kalman filter was reinitialized in eclipse, it did not accept the DSS data when it became available. The algorithm overestimated its accuracy without the DSS data and underestimated the accuracy of the DSS data. Thus it was not as accurate as it could have been if it had used the DSS data. The Kalman filter was re-tuned based on this test in preparation for the Contingency Mode test in Mission Mode.

In reviewing the performance of the Contingency Mode, it was discovered that the magnetic field model on-board was not internally consistent. The coefficients were from a 1995 model, but the epoch time for computation of the secular variations was set to 1990. An attempt was made to update the magnetic field model, but it was discovered that the epoch for the magnetic field model could not be changed using a table load because it was hard coded in the software. The coefficients were set back to correspond to the 1990 epoch for the test in Mission Mode. A software patch was later uploaded to allow the use of the 1995 model.

The Contingency Mode was tested while in Mission Mode after all sensor calibration was complete. The best measure of performance of the Contingency Mode is the attitude derived from the ESA. Although ESA data is not processed while in Contingency Mode, the data is available in telemetry. Figure 7[2] show the attitude errors derived on the ground from ESA telemetry while the spacecraft is controlled to the attitude derived from Contingency Mode. Transients occur when Contingency Mode is entered and when the Kalman filter is reset by the ground during this test. The initial attitude transients are on the order of 1^0 in roll and 0.2^0 in pitch. The steady state performance is on the order of 0.25^0.

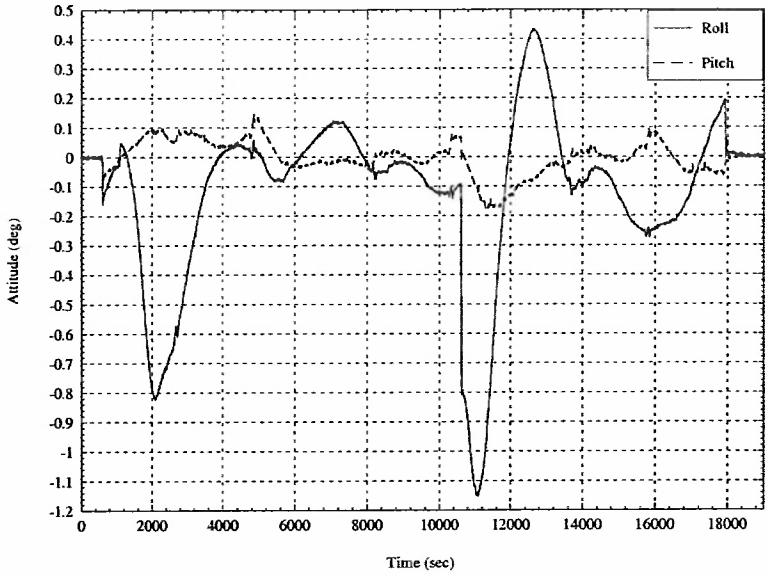

Figure 7 Mission Contingency Mode Test: ESA Attitude

Earth Acquisition

Earth acquisition performance is shown in Figure 8. Within approximately 12 minutes, a nadir attitude was reached and the spacecraft autonomously transitioned to Yaw Acquisition Mode. Mission Mode was autonomously entered within approximately 22 minutes.

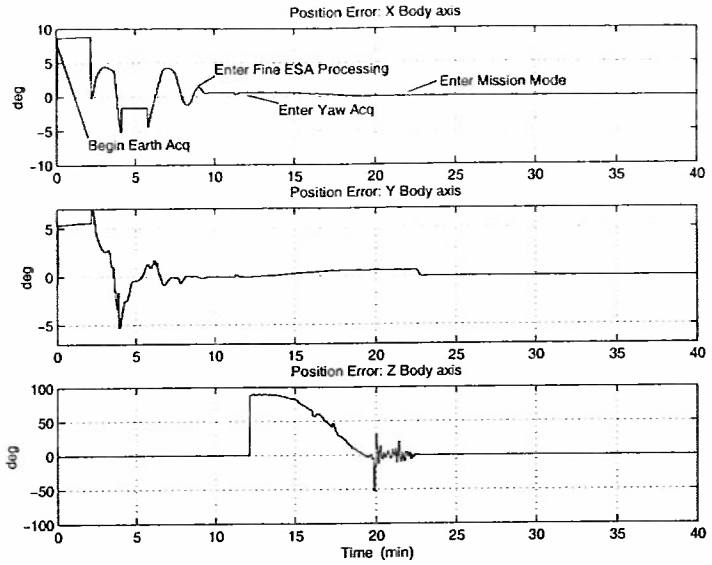

Figure 8 Earth Acquisition: Position Errors

Mission Mode

Upon first entering Mission Mode, the spacecraft attitude showed larger DSS yaw updates than expected. Corresponding to these changes, the on-board estimate of the gyro bias showed similar changes which resulted in significant drift in the yaw direction until the next yaw update. This pattern of attitude fluctuation was traced to not just sensor misalignment but also to a misalignment between the two heads within each DSS. In order to avoid alteration of the flight software, DSS transfer function coefficients were determined to minimize the error due to head misalignment. Figure 9[3] shows how alignment and DSS coefficient uplinks improved the attitude determination performance while in Mission Mode.

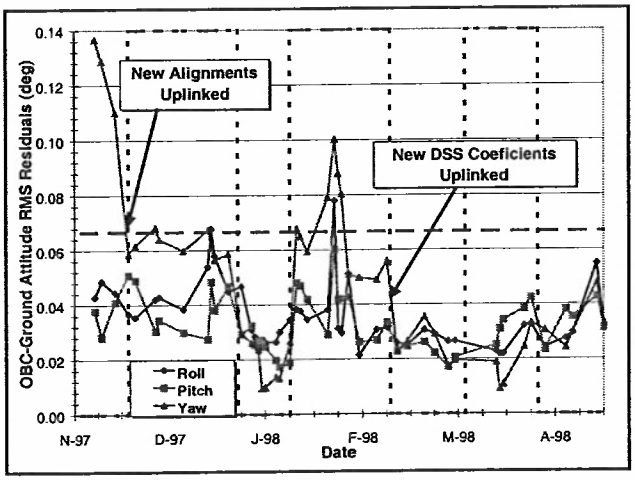

Figure 9 Mission Mode Performance

Another unexpected spike in position error was found to occur in roll and pitch during times of Sun passage through one the ESA quadrant's Field Of View (FOV), as shown in Figure 10. It was determined that these spikes were caused by the on-board ESA processing. When the Sun is predicted to intrude into an ESA quadrant FOV, that quadrant is not used in attitude computations and the output for that quadrant is not filtered. When the Sun is predicted to leave the quadrant FOV, it is then again used in attitude computations and filtering resumes. The spikes in position error resulted from an error in the on-board algorithm which did not reset the filter properly when it was turned back on. The bottom plot in Figure 10 illustrates the position error with filtering turned off during a period of time when the Sun passes through the same ESA quadrant FOV. It can be seen that the removal of the filter has greatly minimized the effect of spikes due to Sun intrusion. A flight software change could be made to correct the filter initialization; however, the performance with the filter turned off was deemed to be adequate.

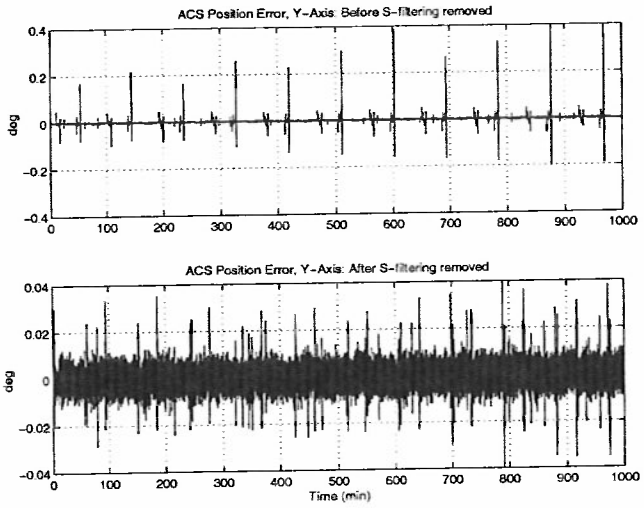

Figure 10 Mission Mode: Position Error

Thruster Calibration and Delta V performance

The TRMM thruster calibration consisted of one-shot firings of each of the 4 roll control thrusters, two 10 second firings of the 4 thrusters located on the ISP, and one 10 second firing of the 4 thrusters located on the LBS. One shot firings consisted of a single 200 msec pulse commanded by the ground. The 10 second ISP and LBS firings were accomplished by entering Delta V Mode.

The ISP thrusters were tested during a 10 second Delta V calibration firing. The Delta V was successful, but the -Pitch thruster was only on for about 7 seconds. A retest resulted in the same performance. Initial simulations predicted that all four Delta V thrusters would be commanded on for the entire 10 seconds. For such a short duration burn it was not believed that the disturbances would cause the attitude errors to reach the switching limits. When these switching limits are reached, the ACS automatically off-

modulates the appropriate thruster. Slight differences in the assumptions for center of mass, thruster alignment, thruster positions, and thrust levels will cause slight variations in the time required to reach the -pitch switching limit. It should be noted that the center of mass is above the X-Y plane, so some net -Pitch torque is expected. The 10 second test of the LBS thrusters resulted in no off-modulation of any of the thrusters. Table 3 gives actual and expected thruster accelerations.

Table 3
THRUSTER ACCELERATIONS

Acceleration	Actual (deg/sec^2)			Expected (deg/sec^2)		
ISP disturbance	-2.99E-06	-6.15E-04	1.39E-05	-9.64E-08	-4.64E-04	7.43E-05
ISP control	-3.46E-06	1.18E-03	-2.88E-05	-4.65E-06	1.01E-03	7.73E-05
ISP-Pitch	4.68E-07	-1.80E-03	4.27E-05	4.56E-06	-1.48E-03	-2.98E-06
LBS disturbance	-9.56E-06	5.32E-04	-9.12E-05	6.84E-06	4.67E-04	-9.65E-05

Although the ISP pitch disturbance acceleration was higher than expected, and the ISP yaw acceleration was almost nonexistent, the controller worked as expected on the actual disturbances. A typical phase plane plot for one of the 3 minute descent burns is shown in Figure 11. The one LBS thruster burn also showed a larger pitch disturbance acceleration than expected, but the yaw disturbance was accurately predicted.

Based on the commanded firing times and the computed thruster accelerations, the ISP -Pitch thruster is off modulated about 34% of the time. The attitude hangs off about 3.4 degrees, which is comparable to the predicted 3.6 degrees. The rate error is controlled to +/- 0.1 deg/sec. The system reaches a steady-state duty cycle in about 60 seconds.

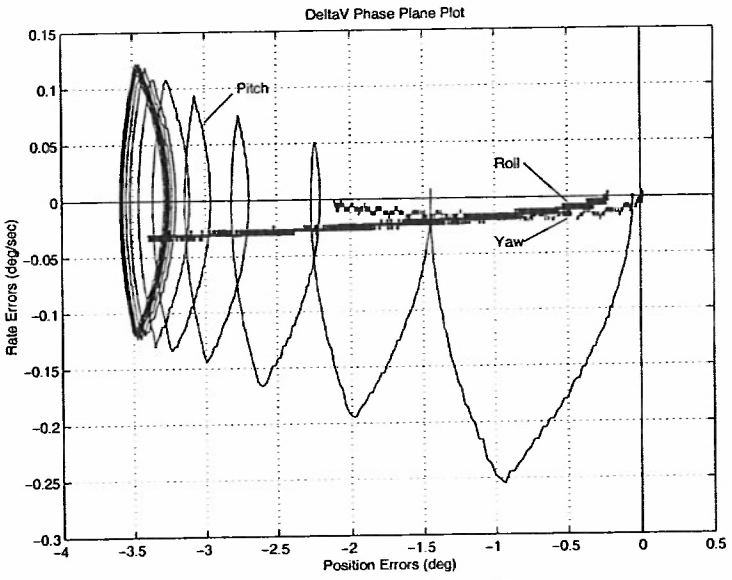

Figure 11 Delta-V Mode: IRU Rate

ON-ORBIT PERFORMANCE

Mission Mode

Once all sensor calibration was complete, the Mission Mode performance was evaluated by performing a ground solution. The ground solution was obtained from a batch least-squares computation of the attitude using all sensor data. The major source of DSS errors was found to be the remaining uncompensated misalignment of the sensor heads. The major source of ESA errors appears to be variation in horizon radiance. The ESA performance was slightly degraded during periods in which one or two of the sensor quadrants could not be used because of the proximity of the Sun or Moon image to the field-of-view. Figure 12 illustrates the ground solution showing performance of the TRMM Mission Mode over a typical orbit. Performance is well within the 0.2^{0} knowledge requirement.

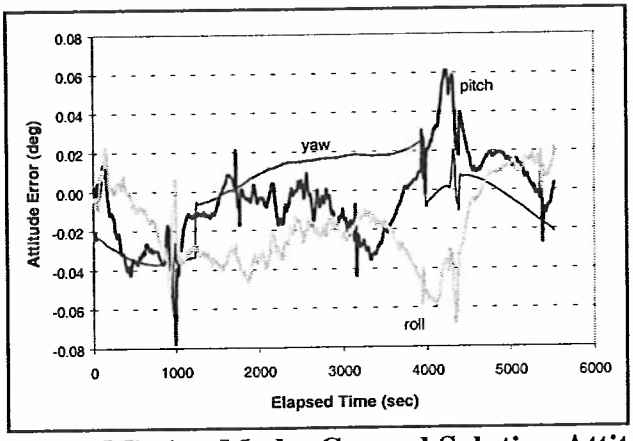

Figure 12 Mission Mode: Ground Solution Attitude

LESSONS LEARNED

A number of lessons learned were derived during on-orbit checkout of the TRMM ACS. One lesson learned deals with the importance of communication between engineers and the importance of allowing flexibility in the ACS flight software. More thorough communication between the ACS and Mechanical engineers could have prevented a misunderstanding of the importance of mounting the DSS heads orthogonal with high precision. More attention during integration and test to the detail of the alignment measurement summary on the part of the ACS team could have identified the problem prior to launch. Finally, the ACS flight software should have been designed with the flexibility to accommodate misalignments of each head rather than each DSS. Extra DSS coefficient tables or alignment matrices for each DSS head would have reduced the amount of effort spent calibrating the DSS post-launch.

Another lesson learned deals with the importance of sensor model fidelity and correlating test data with model assumptions. The autonomous FDC configuration change to the redundant TAM during initial on-orbit operations could have been avoided if a better representation of the TAM noise had been used during design. The post launch removal of the filter in ESA processing could also have been avoided if the thermal dependence of the ESA had been modeled in simulations. The problem with the filter reset when switching from 3 back to 4 quadrant processing was not uncovered because a non-thermally dependent ESA model was used in all simulations and flight software qualification tests. Alternatively, a high fidelity stimulator of the ESA capable of stimulating 3 and 4 quadrant processing could have uncovered the problem during test.

Another lesson learned dealt with the importance of a table design that allows parameters to be changed in flight software without software patches. The DSS misalignment errors were successfully calibrated through table up-link; however, the epoch update for the on-board magnetic field model could not be accomplished without a software patch. Software patches require a significant development and testing effort and impose an additional risk to spacecraft health.

CONCLUSION

The on-orbit performance of the TRMM ACS has been presented along with the mission level requirements. Flight data results show that the TRMM ACS is meeting all of the imposed requirements. Although the TRMM Mission Mode continues to meet pointing requirements and the mission has been very successful to date, lessons learned were realized.

ACKNOWLEDGMENT

The authors wish to thank Marty Frederick, whose leadership of the TRMM ACS effort was a major factor in its success.

REFERENCES

1. "TRMM Attitude Control System Specification", TRMM-712-046, January 31, 1992.

2. S. Andrews and W. Morgenstern, "Initial Flight Results of the TRMM Kalman Filter", Flight Mechanics Symposium, May 1998.

3. B. Robertson et. al., "On-orbit Performance of the TRMM Mission Mode", 14th International Symposium on Space Flight Dynamics, February, 1999.

On-Orbit Performance of the TRMM Mission Mode

Brent Robertson, Sam Placanica, Wendy Morgenstern
NASA Goddard Space Flight Center

Joseph A. Hashmall, Jonathan Glickman, Gregory Natanson
Computer Sciences Corporation

Contact: Brent Robertson
e-mail: brent.robertson@gsfc.nasa.gov
phone: (301) 286-6392

Abstract

This paper presents an overview of the Tropical Rainfall Measuring Mission (TRMM) Attitude Control System along with detailed in-flight performance results of the TRMM Mission Mode. TRMM is a joint mission between NASA and the National Space Development Agency of Japan designed to monitor and study tropical rainfall and the associated release of energy. The TRMM spacecraft is an Earth-pointed, zero momentum bias satellite launched on November 27, 1997 from Tanegashima Space Center, Japan. Prior to calibration, the spacecraft attitude showed larger Sun sensor yaw updates than expected. This was traced to not just sensor misalignment but also to a misalignment between the two heads within each Sun sensor. In order to avoid alteration of the flight software, Sun sensor transfer function coefficients were determined to minimize the error due to head misalignment. This paper describes the design, on-orbit checkout, calibration and performance of the TRMM Mission Mode with respect to the mission level requirements.

TRMM Mission Overview

TRMM is a joint mission between NASA and the National Space Development Agency (NASDA) of Japan designed to monitor and study tropical rainfall and the associated release of energy shaping both weather and climate around the globe. TRMM is the first mission dedicated to measuring rainfall through five microwave and visible infrared sensors, including the first spaceborne rain radar. Launched to provide a validation for poorly known rainfall data sets generated by global climate models, TRMM has demonstrated its utility by reducing uncertainties in global rainfall measurements by a factor of two. A sample image taken by one of the TRMM instruments is shown in Figure 1.

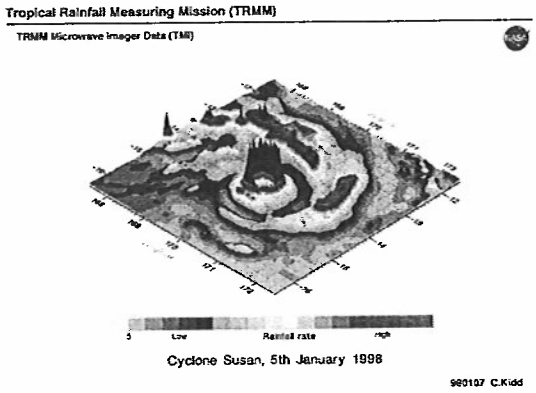

Figure 1: TRMM Science Image

The TRMM spacecraft, shown in Figure 2, was launched on the H-II Expendable Launch Vehicle on November 27, 1997 from Tanegashima Space Center, Japan. The spacecraft is three-axis stabilized, in a near circular 350 km orbit with inclination of 35^{o}. At launch, the spacecraft had a mass of 3,523 kg including 903 kg of fuel and pressurant.

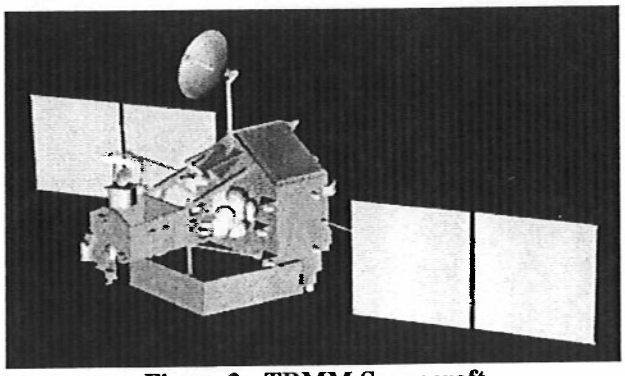

Figure 2: TRMM Spacecraft

TRMM Attitude Control System Design

The TRMM Attitude Control System (ACS) Mission Mode is required to maintain a nadir pointing attitude

with requirements shown in Table 1[1]. Since the science requirement did not specify either a geocentric or geodetic reference, for convenience the nadir reference was defined by the output of the chosen Earth Sensor Assembly (ESA). This resulted in a nadir reference (Z) defined by a horizon bisector of the CO_2 horizon of the Earth, so that spacecraft pointing is provided with respect to a quasi-geodetic position. Analysis shows that this reference frame is approximately 0.01^0 from the geodetic frame with nominal ESA performance.

Table 1: ACS Mission Mode Pointing Requirements

Characteristic	Requirement (per axis)
Pointing Knowledge, on-board (3σ)	0.2^0
Pointing Accuracy (3σ)	0.4^0
Stability (peak to peak)	0.1^0 over 1 sec

Due to an instrument thermal requirement that the +Y side of the spacecraft stay cold, the Mission Mode is required to operate in either a +X forward or –X forward orientation. The spacecraft is commanded to rotate 180^0 about nadir (yaw) every few weeks when the Sun crosses the orbit plane. Due to these yaw rotations, the spacecraft maintains an angle between the Sun and the spacecraft X-Z plane of between 0^0 and 58.4^0.

The TRMM ACS architecture is shown in Figure 3. The ACS is comprised of Attitude Control Electronics (ACE), an ESA, Digital Sun Sensors (DSS), Inertial Reference Units (IRU), Three-Axis Magnetometers (TAM), Coarse Sun Sensors (CSS), Magnetic Torquer Bars (MTB), Reaction Wheel Assemblies (RWA), Engine Valve Drivers (EVD) and thrusters. The ACE is comprised of an 80C86 processor, DC-DC converters, and actuator and sensor interface electronics. The ACE processor formats raw sensor data, decodes commands and contains Safe Hold flight software. The ACE transmits the sensor data over a 1773 fiber optics data bus to the ACS processor to be used by the ACS software and down-linked in telemetry. The flight software for initialization, attitude determination and control, momentum management, ephemeris generation, solar array commanding, High Gain Antenna (HGA) commanding, mode management and Fault Detection and Correction (FDC) are implemented in the ACS Processor. The FDC software provides tolerance of a single point failure with minimal interruption to science data gathering. The computed control torques are sent back to the ACE, which relays the appropriate commands to the actuators. The TRMM ACS operates at a 2 Hz control rate while in Mission Mode. All TRMM ACS components are fully redundant and cross-strapped with the exception of the MTBs which have redundant windings that are not cross-strapped.

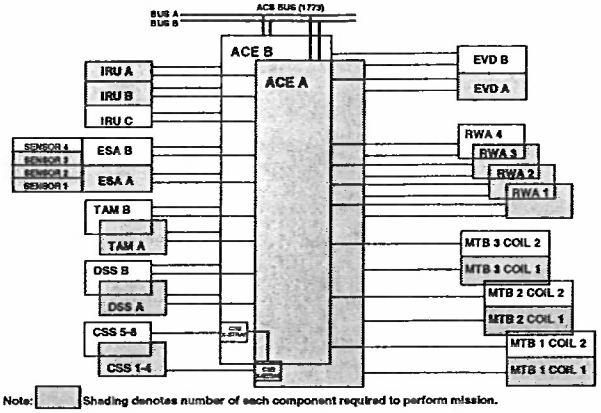

Figure 3: ACS Architecture

The ACS Mission Mode utilizes a static ESA, two DSS's and IRUs for attitude sensing. The ESA provides roll (X) and pitch (Y) axis attitude error measurements. Yaw (Z) position is determined with DSS updates and propagated between updates using gyro output. Four RWAs arranged in a pyramid configuration are used for control. The TAM and three MTBs are used for momentum management. A simple Proportional-Integral-Differential (PID) controller is used in Mission Mode, as shown in Figures 4 and 5.

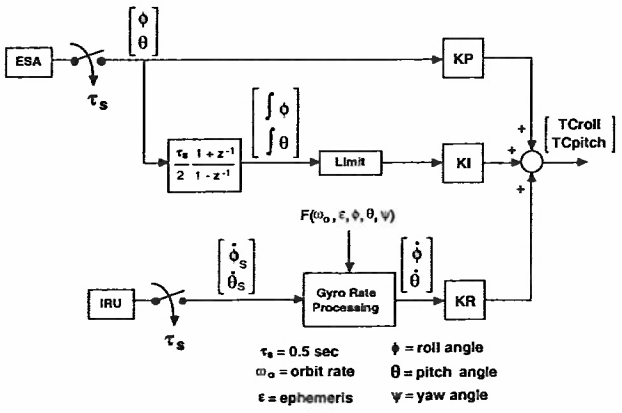

Figure 4: Mission Mode Roll / Pitch Controller

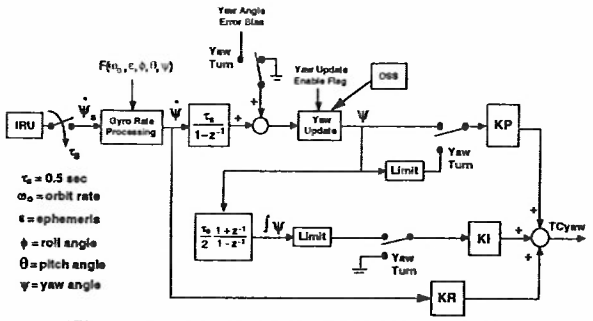

Figure 5: Mission Mode Yaw Controller

The ESA used on TRMM is an infrared horizon sensor with no moving parts. The ESA independently views segments of the horizon in the centers of the North-East, North-West, South-East, and South-West quadrants. Each quadrant contains four detectors, three of which are nominally in view of the Earth limb. The fourth detector, known as the S detector, is nominally in view of cold space and provides a space radiation measurement.

Each of the DSS's has a pair of heads mounted orthogonally to provide two axes of information. Each head senses the Sun angle in a single axis over a 96^0 Field Of View (FOV) about the head bore-sight axis. Twice an orbit, the DSS readings are compared to an ephemeris-based expected reading to provide an attitude reference for the yaw axis gyro as well as a new yaw gyro bias. One DSS looks in a forward (+X) direction and another points in the aft (-X) direction, as shown in Figure 6. The bore-sight orientations were chosen so as to maximize the time during which DSS data was available.

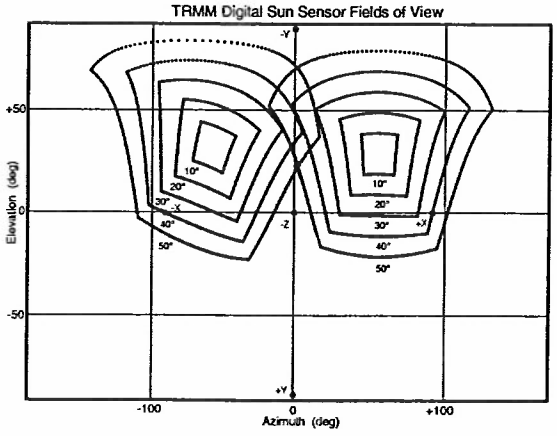

Figure 6: TRMM DSS Field of View

On-Orbit Checkout

On-orbit checkout of the TRMM Mission Mode uncovered two unexpected performance features. Both anomalies were dealt with by uploading new table values in the ACS flight software.

Soon after launch, a significant inconsistency between the output of the DSS's was found. Consequently, each on-board yaw attitude update resulted in a significant attitude change. The yaw measurement from one DSS was inconsistent with the previous update, from the other DSS. The spacecraft compensated by maneuvering to null the new yaw measurement and computing a new gyro bias, based on spacecraft attitude motion assumed to be equal to the difference between the two DSS yaw measurements. The new gyro bias was used to control the spacecraft until the next yaw update, resulting in a larger update.

The cycle of DSS and gyro bias correction on-board resulted in the spacecraft attitude developing the pattern shown in Figure 7. The ground solution is obtained by gyro propagation of the epoch attitude from a batch least-squares computation using a full orbit's sensor data. Batch processing of this amount of data results in an attitude that uses all of the data and therefore is more accurate than an instantaneous sensor measurement.

The ACS drives the on-board computed attitude errors to zero. The On-Board Computer (OBC) attitude therefore shows constant, near zero attitudes except at each yaw update. When a new inconsistent DSS measurement shows a yaw deviation, the spacecraft maneuvers to remove it. This results in a brief spike in the OBC yaw attitude.

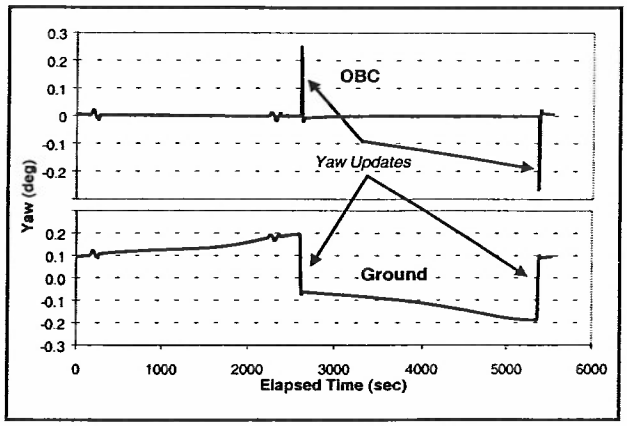

Figure 7: Pre-calibration Yaw Attitude

The spikes in the yaw position were found to be caused by a misalignment of the two DSS heads with respect to each other. The flight software assumed that the DSS heads would be mounted orthogonal to each other, when in fact a review of alignment records indicated that the heads were only mounted orthogonal to within approximately 0.2^0. The effect of this misalignment on attitude performance was minimized post-launch through sensor calibration, as described in the next section.

Another unexpected spike in position error was found to occur in roll and pitch during periods of time when the Sun was in one the ESA quadrant's FOV. The top plot in Figure 8 shows spikes in the pitch position error which correspond to Sun passage through one of the ESA quadrant's FOV. It was determined that these spikes were caused by the on-board ESA processing. The S detector output is filtered by the on-board software. When the Sun is predicted to intrude into a quadrant FOV, that quadrant is not used in attitude computations and the S detector for that quadrant is not filtered. When the Sun is predicted to leave the quadrant FOV, it is then again used in attitude computations and filtering of the S detector resumes.

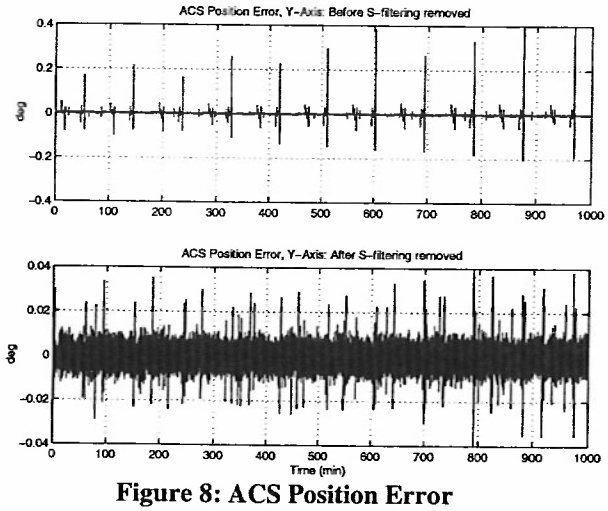

Figure 8: ACS Position Error

The spikes in position error resulted from an error in the on-board algorithm which did not reset the S filter properly when it was turned back on. The spikes are the dynamical response of the filter as it settles after this sudden jump in data. The bottom plot in Figure 8 illustrates the position error with S filtering turned off during a period of time when the Sun passes through the same ESA quadrant FOV. It can be seen that the removal of the S filter has greatly minimized the effect of spikes due to Sun intrusion. A flight software change could be made to correct the S filter initialization; however, the performance with the S filter turned off was deemed to be adequate.

Sensor Calibration and Attitude Validation

The TRMM attitude sensors were calibrated after launch in order to improve on-orbit performance. The relative alignment of the ESA and the two DSS's were determined to improve attitude consistency. Changes in the DSS transfer function coefficients were determined in order to compensate for the non-orthogonality of the DSS heads. The gyros were calibrated to improve the targeting accuracy of slew maneuvers. Because the magnetometers are only used for attitude determination in a contingency mode, their calibration is not described here.

Alignment Calibration: Alignment calibration is performed on orbit to insure that the computed attitude is consistent, regardless of which sensors are used as input and regardless of the relative amounts of data received from each sensor. For TRMM, on-board roll and pitch were taken directly from the ESA while yaw was taken from the two DSS's. Ground computation of attitude was performed by a batch-least squares algorithm using input from both of the DSS's, the ESA and the gyros.

A portion of the attitude inconsistencies was found to have been caused by misalignment of the DSS's and the ESA relative to each other. The effect of the misalignment of the DSS's was removed by determining a misalignment matrix, **M**, and applying it to the raw DSS vectors before applying the nominal alignment transformation, **N**, to transform these vectors from the sensor to the body frame.

$$\hat{O}_{body} = N_{\text{nominal\_to\_body}}\, M_{\text{true\_to\_nominal}} \hat{O}_{observed} \qquad (1)$$

The misalignment matrices, M, were determined using two algorithms that gave similar results. Both used all sensor data in a batch least-squares algorithm to minimize a Wahba loss function:

$$\mathcal{L} = \sum_{t,i} W_i \left[A_t \hat{R}_{t,i} - N_i M_i \hat{O}_{t,i} \right]^2 \qquad (2)$$

where the A_t is the attitude at time t, N_I, $\mathbf{M}_I$, and W_I the nominal alignment, misalignment matrix and weight for sensor I, and $\mathbf{O}_{t,I}$ and $R_{t,I}$ are observation and reference vectors from sensor I at time t.

The misalignment of the ESA was parameterized in terms of penetration angle biases. These biases are the difference from nominal that the Earth horizon penetrates into individual single quadrants when the pitch and roll are zero. Differences between penetration angle biases on opposite quadrants are equivalent to misalignment angles.

The first algorithm minimized this loss function with respect to a state vector including an epoch attitude, gyro biases, and misalignment parameters. The second algorithm minimized the same loss function with respect to only the epoch attitude and gyro biases (keeping a identity misalignment matrices for all three sensors and zero penetration biases for the ESA) to produce a reference attitude and gyro biases. A second step was then used to minimize the loss function (using the gyro-propagated attitude from the first step) with respect to the misalignment parameters.

Both of these algorithms give relative alignments because a misalignment corresponding to the rotation of all of the sensors together is inherently unobservable. Before launch it had been decided that DSS-2 would be used as the reference sensor. The specific misalignments were to be determined so that the misalignment of DSS-2 would be identity. This choice was made because mechanical analysis indicated that DSS-2 would be less likely to shift at launch than DSS-1. The second cause of the attitude behavior shown in Figure 7 was due to the two heads of each DSS not being mounted orthogonal to each other. Because this misalignment was smaller for DSS-1, the reference was changed to DSS-1.

Using $\mathbf{M}_{DSS\text{-}1} = \mathbf{I}$, the misalignment matrices of DSS-2 and penetration angle biases of the ESA were found to be:

$$M_{DSS-2} = \begin{bmatrix} 999.996 & -1.98736 & -1.99437 \\ 1.99280 & 999.994 & 2.72920 \\ 1.98893 & -2.73316 & 999.994 \end{bmatrix} \times 10^{-3} \qquad (3)$$

$$b_{ESA} = \begin{bmatrix} -0.1574 \\ 0.04635 \\ -0.09414 \\ -.05382 \end{bmatrix} \text{degrees}$$

Figure 9 shows the root-mean-square (RMS) differences between OBC and ground batch least-squares attitudes computed for the first several months of the mission. Because the ground solutions use all of the data, including gyro data, they are more accurate than the OBC attitudes and this figure can be considered to be a plot of OBC attitude errors. The six vertical dotted lines are drawn (on this and on the two subsequent figures) at the times when TRMM had 180^0 yaw maneuvers to change its orientation with respect to the Sun. As can be seen from the figure, uplink of the new alignments significantly reduced the OBC attitude error.

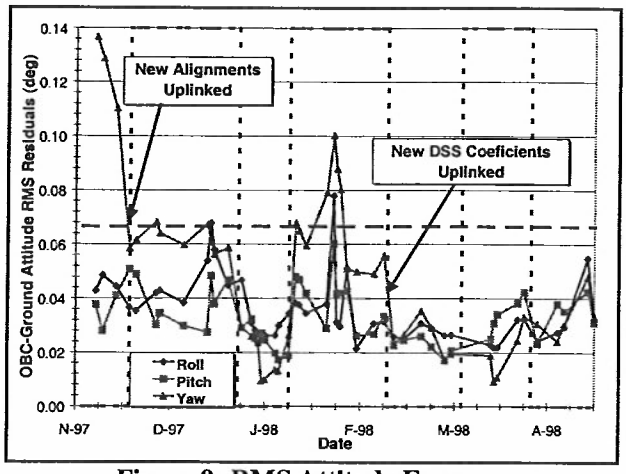

Figure 9: RMS Attitude Error

The horizontal dashed line in Figure 9 represents the required (1σ) TRMM attitude accuracy.

Figure 10 shows the effect of calibration on the size of the yaw update throughout the early mission. Uplink of the new alignments significantly decreased the size of the yaw update.

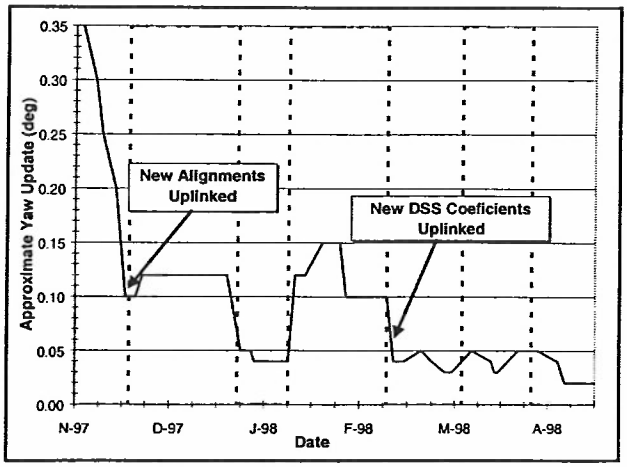

Figure 10: Yaw Update

DSS Transfer Function Calibration: A major cause of the attitude inconsistency resulting in the behavior shown in the figures above was non-orthogonality of the DSS heads. Each DSS contains two heads that measure angles in two, nominally orthogonal, directions. These two angles, α and β, are converted to an observed Sun unit vector in the sensor frame by:

$$\hat{O}_{\text{Sun}} = \begin{bmatrix} \tan\alpha \\ \tan\beta \\ 1 \end{bmatrix} \left(\tan^2\alpha + \tan^2\beta + 1\right)^{-1/2} \qquad (4)$$

Analysis of the large attitude changes at each yaw update led to an investigation of the prelaunch head mounting geometry. The α and β heads of both sensors (especially DSS-2) were mounted at an angle with significant misalignments. If the orientation of the β head is represented as a 2-3-1 Euler sequence, the rotation angles of DSS-1 were 0.044, -0.008, and 0.067 deg while those of DSS-2 were 0.206, 0.061, and 0.182 deg.

Unfortunately, the on-board attitude software, the ground attitude determination software, and the sensor calibration software were not designed to determine or use non-orthogonal misalignment matrices.

Three factors existed that allowed for a relatively simple and effective compensation for the DSS head non-orthogonality. The DSS data was only used to update yaw attitudes at one specific value of α in each DSS, the calibration software was capable of determining new transfer function coefficients for the DSS's, and the on-board software was capable of using these new coefficients.

The DSS α and β observations are generated from raw output of the two heads, N_α and N_β, by:

$$\alpha = \tan^{-1}\left[\begin{matrix} a_1 + a_2 N_\alpha + a_3 \sin\left(a_4 N_\alpha + a_5\right) \\ + a_6 \sin\left(a_7 N_\alpha + a_8\right) \end{matrix}\right] + a_9$$

$$\beta = \tan^{-1}\left[\begin{matrix} b_1 + b_2 N_\beta + b_3 \sin\left(b_4 N_\beta + b_5\right) \\ + b_6 \sin\left(b_7 N_\beta + b_8\right) \end{matrix}\right] + b_9 \qquad (5)$$

Non-orthogonality of the DSS heads resulted in a formal dependence of transfer function coefficients on the position of the Sun relative to the sensor boresight. It was suggested that this dependence could be compensated using new values of the coefficients that minimized errors at the time of each yaw update. To eliminate the dependence of the a-coefficients on the position of the Sun, the α axis of each sensor was taken as its reference axis. Because the yaw updates always occur when the Sun vector intersected the XY body plane, minimum error β values were obtained using b-coefficients given by:

$$\begin{aligned} b_1' &= cb_1 + d \\ b_i' &= cb_i \quad i = 2,3,6 \end{aligned} \qquad (6)$$

Based on pre-launch head misalignments, the resulting values of ***c*** and ***d*** were 1.000047 and 0.000085 for DSS-1 and 0.999977 and 0.000053 for DSS-2.

As can be seen in Figures 9 and 10, the use of these new coefficients (after February 27, 1998) decreased both the attitude error and size of the yaw update. An interesting, but unexplained, observation is that before uplink of these coefficients the yaw attitude was more accurate, and the yaw updates smaller, in the +X forward configuration than in the –X forward configuration. After uplink of the coefficients the values were small in both configurations.

Gyro Calibration: Calibration of spacecraft gyros does not affect the accuracy of spacecraft attitudes as long as the attitude solution method contains gyro biases in its state vector and the spacecraft rates are approximately constant as they are in Mission Mode. Gyro calibration is performed in order to improve the accuracy of maneuver targeting.

Raw gyro rates, ω_0, are converted to adjusted rates by:

$$\begin{aligned} \vec{\omega} &= G\vec{\omega}_0 + \vec{b} \\ G &= MS \end{aligned} \qquad (7)$$

where ***M*** is a true normalized misalignment matrix, ***S*** a diagonal scale factor matrix, ***G*** the product of the two (not orthonormal) and ***b*** a bias vector. Using an a priori values of $\boldsymbol{G} = \boldsymbol{I}$ and assuming ω_0 is nearly constant:

$$\begin{aligned} &\vec{\omega} = \vec{\omega}_0 + \vec{b}' \quad \text{where} \\ &\vec{b}' = \vec{b} + \left(MS - I\right)\vec{\omega}_0 \end{aligned} \qquad (8)$$

where $\vec{b}'$ is the ***solved for*** bias vector.

During attitude maneuvers, rates are not constant so the attitude change during a maneuver from t_0 to t depends on the misalignment matrix, scale factors, and bias vector.

Gyro misalignments, scale factors, and biases were determined using a transition-matrix version[2] of the Davenport method[3,4]. This method requires data from at least four separate intervals in which the integrated rate vectors are linearly independent. For TRMM, an interval in normal Mission Mode, an interval during a 180^0 yaw maneuver, and intervals during CERES and Precipitation Radar (PR) calibration maneuvers were used.

To use the Davenport algorithm, reference attitudes at times immediately before and after each calibration period were computed using data from constant rate periods before and after each maneuver. Because TRMM rates were constant during these periods, accurate reference attitudes could be obtained at each of these times. The attitude at the end of each calibration period depends not only on the attitude at the start but also on the gyro misalignments, scale factors, and biases. Values for these parameters were found that minimized the differences between reference attitudes and propagated attitudes at the end of each interval. The propagated attitudes were computed by propagation of the reference attitude at the start of each interval using gyro data adjusted with the misalignments, scale factors and biases.

The results of the calibration were:

$$G = \begin{bmatrix} 1.000443 & -1.01300\times10^{-3} & 6.75235\times10^{-4} \\ 7.63599\times10^{-4} & 1.00053 & -2.1629\times10^{-3} \\ 9.41394\times10^{-4} & 1.6831\times10^{-3} & 1.00088 \end{bmatrix} \quad (9)$$

$$\vec{b} = \begin{bmatrix} -1.549155 \\ 1.978161 \\ 0.7820254 \end{bmatrix} \times 10^{-4} \text{ deg/sec}$$

The calibration success was evident in two ways. Targeting of the 180^0 yaw maneuvers became significantly more accurate in all three axes. The error in yaw, pitch, and roll attitudes after a 180^0 yaw maneuver are shown in Table 2. This table gives figures for the same yaw maneuver propagated using the precalibration and postcalibration gyro parameters. Note that, probably due to misalignment, the roll attitude was significantly in error before calibration, and that this error was dramatically reduced by the calibration.

Table 2: Yaw Maneuver Attitude Error (deg)

Attitude Component	Precalibration Error	Postcalibration Error
Yaw	-0.096830	-0.044520
Pitch	0.010712	0.005767
Roll	0.248440	-0.005775

The increase in targeting accuracy is especially important for TRMM because the on-board attitude determination accepts yaw input only twice each orbit. A significant period might therefore elapse between the end of a yaw maneuver and the next yaw attitude update. During this period TRMM would have significant attitude error.

If the calibration parameters are correct, the bias vector solved for using the normal attitude determination methods should be independent of the (nearly constant) rates. TRMM pitches at ±1 revolution per orbit (RPO) depending on whether it is flying +X forward or –X forward. Differences between the apparent gyro biases computed while it rotates at either + or –1 RPO shows the calibration accuracy. A plot of gyro biases during the first 5 months of operation is shown in Figure 11. The variation in gyro bias depending on TRMM orientation is clearly evident before the uplink of the gyro calibration parameters. For the first maneuver (on March 21, 1998) after these parameters were applied the computed gyro biases became nearly independent of TRMM orientation.

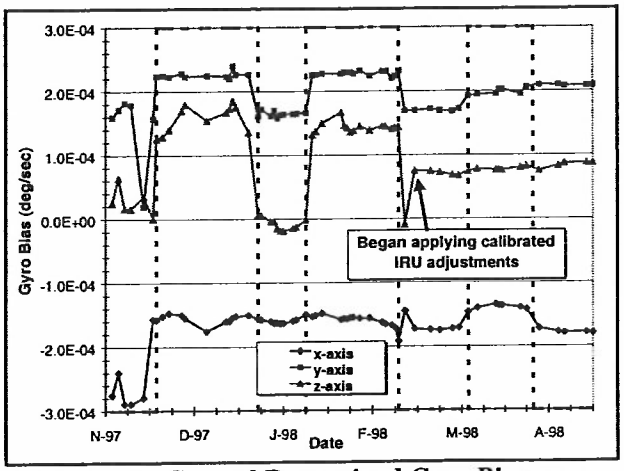

Figure 11: Ground Determined Gyro Biases

On-orbit Performance: The attitude performance of TRMM Mission Mode is summarized in Table 3.

In this table three measures of performance are displayed: attitude accuracy, yaw update, and the standard deviation of the gyro bias. The attitude accuracy is the average over the period of RMS differences between batch least-squares ground attitudes and the OBC attitudes. Each RMS difference is taken over at least a full orbit of data. The yaw updates are an average of the attitude change that occurred each time the yaw attitude was updated on-board. The standard deviations of gyro biases show how stable the biases were during each period.

The periods used for performance evaluation were

- Precalibration: Launch to December 11 (before any calibration parameters were uplinked)
- Calibration 1: December 11 to February 28 (after alignment calibration values were uplinked)
- Postcalibration: All of March and April (period after the DSS FOV coefficients and gyro calibration parameters were uplinked)

For the gyro bias parameters only two periods are used corresponding to the second and third of those used for the other parameters.

Table 3: TRMM Mission Mode Attitude Performance

Parameter	Axis	Pre-calibration	Calibration -1	Post-calibration
Attitude Accuracy (deg)	Roll	0.045	0.038	0.029
	Pitch	0.036	0.035	0.030
	Yaw	0.130	0.051	0.026
Yaw Update (deg)		0.24	0.10	0.04
Gyro Bias Standard Deviation (deg/hour)	X	0.0312		0.0668
	Y	0.1046		0.0579
	Z	0.2675		0.0214

Calibration of the attitude sensors and gyros significantly improved TRMM attitude performance. Before calibration the yaw attitude did not meet mission requirements while after calibration it fell well within requirements. The mitigation of the unexpected yaw updates was particularly gratifying. The decrease in the size of yaw updates is easily seen by comparing the precalibration ground and on-board attitudes in Figure 7 with the corresponding postcalibration values in Figure 12.

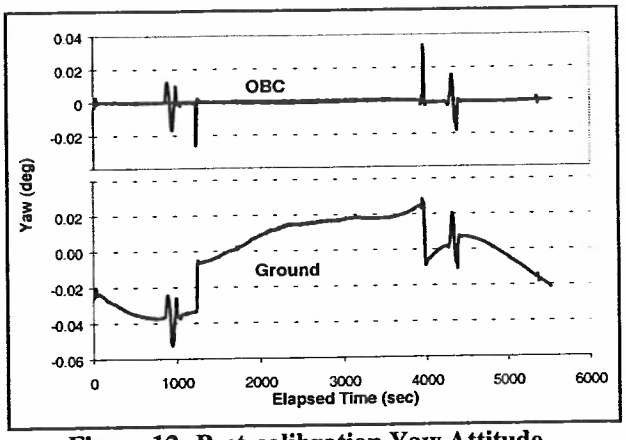

Figure 12: Post-calibration Yaw Attitude

The postcalibration attitude error for TRMM, over a full orbit, is shown in Figure 13.

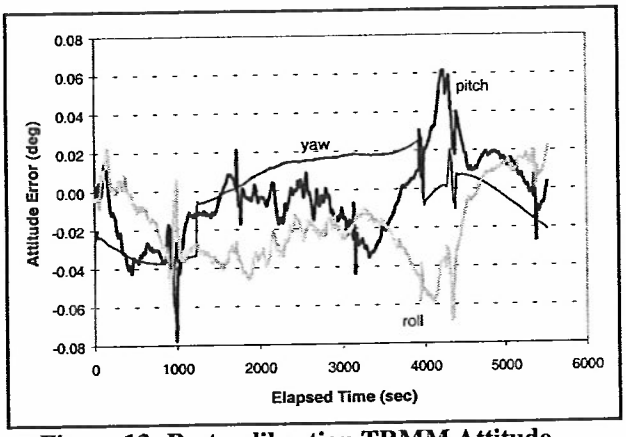

Figure 13: Post-calibration TRMM Attitude

Conclusion

The on-orbit performance of the TRMM ACS has been presented along with the mission level requirements. Flight data results show that the TRMM ACS is meeting all of the imposed requirements after sensor calibration. Lessons learned were realized during on-orbit checkout and sensor calibration.

The obvious lesson learned deals with the nonorthogonal mounting of the DSS heads. This lesson learned deals with the importance of communication between engineers and the importance of allowing flexibility in the ACS flight software. More thorough communication between the ACS and Mechanical engineers could have prevented a misunderstanding of

the importance of mounting the heads orthogonal with high precision. More attention during integration to the detail of the alignment measurement summary on the part of the ACS team could have identified the problem prior to launch. Finally, the ACS flight software should have been designed with the flexibility to accommodate misalignments of each head rather than each DSS. The flight software should have been designed to have alignment matrices or coefficients that could be uploaded to accommodate misalignments between heads.

Another lesson learned deals with the importance of sensor model fidelity. The post launch removal of the S filter in ESA processing could have been avoided if the thermal dependence of the ESA had been modeled in simulations. The problem with the S filter initial condition when switching from 3 back to 4 quadrant processing was not uncovered because a non-thermally dependent ESA model was used in all simulations and flight software qualification tests. Alternatively, a high fidelity stimulator of the ESA capable of stimulating 3 and 4 quadrant processing could have uncovered the problem during test.

Acknowledgements

The authors wish to thank Marty Frederick, whose leadership of the TRMM ACS effort was a major factor in its success, and Mr. James Kast (CSC) for analysis of the pre-launch DSS coefficients. This work was supported, in part, by the National Aeronautics and Space Administration/ Goddard Space Flight Center, Greenbelt, MD USA, Contract GS-35F-4381G, Task Order no. S-03365-Y.

References

1. "TRMM Attitude Control System Specification," TRMM-712-046, January 31, 1992.

2. G. Natanson, "A Transition Matrix Approach to the Davenport Gyro Calibration Scheme," *Proceedings of the 13th International Symposium on Space Flight Dynamics,* NASA Conference Publication AAS 98-335, Greenbelt, MD, May 1998, pp. 373–388.

3. P. Davenport, *In-flight Calibration of Gyros*, Goddard Space Flight Center, Spring 1976

4. J. Keat, *Gyro Calibration Analysis for the High Energy Astronomy Observatory-A (HEAO-A)*, CSC/TM-77/6082, prepared by Computer Sciences Corporation, June 1977

AIAA-98-4509

DESIGN, IMPLEMENTATION, TESTING, AND FLIGHT RESULTS OF THE TRMM KALMAN FILTER

Stephen F. Andrews*
Goddard Space Flight Center, Code 572
Greenbelt, MD, 20771

Wendy M. Morgenstern†
Goddard Space Flight Center, Code 572
Greenbelt, MD, 20771

Abstract

The Tropical Rainfall Measuring Mission (TRMM) spacecraft is a nadir pointing spacecraft that nominally controls attitude based on the Earth Sensor Assembly (ESA) output. After a potential single point failure in the ESA was identified, a backup attitude determination method was designed employing a sixth-order extended Kalman filter using digital sun sensor and magnetometer measurements to update the attitude and the gyro biases. This algorithm was added to previously-tested flight code, and many software verification tests were required to ensure that both the new and the original software requirements were still met. TRMM was launched November 27, 1997, and the Kalman filter algorithm was run twice as part of the in-orbit checkout procedures. This paper provides an overview of the design, implementation, and testing of the TRMM Kalman filter. In addition, initial flight results and some lessons learned are presented.

Introduction

The Tropical Rainfall Measuring Mission (TRMM) spacecraft is a joint NASA/NASDA mission that was launched on November 27, 1997 from Tanegashima Space Center, Japan. The spacecraft is three-axis stabilized, in a near circular 350 km orbit at 35° inclination. The sensor complement includes a static Earth Sensor Assembly (ESA), two two-axis Digital Sun Sensors (DSS), a redundant Inertial Rate Unit (IRU), eight Coarse Sun Sensors (CSS), and two Three-Axis Magnetometers (TAM). The spacecraft will be controlled with four Reaction Wheels (RW), twelve thrusters (Reaction Engine Modules, REM), and momentum will be unloaded with three Magnetic Torquer Bars (MTB). In Mission Mode, which is the nadir pointing science configuration, attitude determination is done with the ESA for roll and pitch, and integrated IRU rate for yaw.

* Aerospace Engineer, Guidance, Navigation, and Control Center.
† Aerospace Engineer, Guidance, Navigation and Control Center. Member, AIAA.

Problem Description

A potential single point failure of the ESA was first detected at Goddard Space Flight Center (GSFC) in 1992, with the discovery of a "fogging" effect of the ESA lenses.[1] This effect could cause the ESA to fail the attitude determination requirement during the nominal Mission Mode. A backup attitude determination method was needed to satisfy the redundancy requirements. Buying another ESA or a Star Tracker (ST) was not a realistic option, given the TRMM budget and schedule. A software backup using the available sensor measurement added redundancy without requiring additional hardware or affecting other subsystems such as power or structures.

Algorithm Heritage

Solar, Anomalous, Magnetospheric Particle Explorer (SAMPEX) uses a DSS and a TAM to calculate a deterministic attitude solution employing a TRIAD algorithm.[2] For estimation attitude determination, typical spacecraft applications of a Kalman filter use a DSS and a Star Tracker (ST) to update the IRU propagated attitude. The Solar Maximum Mission (SMM), the Extreme Ultra Violet Explorer (EUVE), and the Rossi X-ray Timing Explorer (RXTE) use a Kalman filter with a DSS and a ST, for example.

Hashmall, Rokni, and Sedlak first demonstrated the feasibility of determining spacecraft attitude using only magnetometer and gyro data.[3] Their analysis, based on flight data from the Upper Atmosphere Research Satellite (UARS) and the Extreme Ultra Violet Explorer (EUVE), showed that magnetometers, with gyros, could be used to determine attitude to an accuracy of less than 0.1°, 1σ. This study, coupled with flight heritage, gave GSFC the confidence to design a contingency attitude determination mode utilizing the existing gyros, TAM and DSSs as backup attitude sensors.

A trade study was done to determine which attitude determination algorithm would be added to the TRMM software. Several contingency attitude determination algorithms were evaluated for accuracy, code size, telemetry requirements, and amount of additional software needed to support the new algorithm. Based on the results of a trade study, a six state Kalman filter was chosen to backup the ESA.[2] The top-level attitude knowledge requirement on this backup attitude determination algorithm is 0.7° (3σ) per axis, which is the maximum attitude determination error the scientists can tolerate. The filter provides updates to the IRU propagated attitude and the IRU drift rate biases with TAM and DSS measurements.

The TRMM Kalman filter was adapted from RXTE Kalman filter, which was based on the Kalman filter developed for the Multimission Modular Spacecraft (MMS) by Murrell[4], and described in Lefferts, Markley, and Shuster.[5] The major changes to the RXTE algorithm were the replacement of ST processing with TAM processing, the addition of a second DSS, and the coding of new interfaces to fit the algorithm into the existing, tested flight code. Since the core part of the Kalman filter code was already tested and working in flight on RXTE, there was a high degree of confidence in it which allowed a 'black box' testing approach to the new algorithm.

Algorithm Development

The core Kalman filter algorithm on board TRMM was taken from the RXTE algorithm documentation. The main portion of the algorithm is a discrete, extended Kalman filter. It uses the formulation for covariance propagation, Kalman gain calculation, state estimate update and covariance update given in Gelb.[6]

System Model

The TRMM Kalman filter has a six component state vector: $\underline{x} = [\underline{\delta\theta} \quad \underline{\Delta b}]^T$ where $\underline{\delta\theta}$ denotes the three attitude error angles and $\underline{\Delta b}$, are the three gyro bias errors. In the ensuing discussion, the ^ notation indicates an estimated quantity, and the subscript k or k-1 indicates the relevant computer cycle of interest. The TRMM Kalman filter algorithm uses the gyro dynamics equations derived by Farrenkopf[7] to model the evolution of the gyro bias errors, $\underline{\Delta b}$. The spacecraft attitude quaternion, q_{Ib}, represents the true orientation of the spacecraft body axes with respect to the geocentric inertial frame. The kinematics equations of motion are derived from the spacecraft's estimated body rates as measured by the gyros, $\underline{\hat{\omega}} = [\hat{\omega}_1 \quad \hat{\omega}_2 \quad \hat{\omega}_3]^T$, using the equations

$$\dot{q}_{I\hat{b}} = \frac{1}{2}\Omega(\underline{\hat{\omega}})q_{I\hat{b}} \tag{1}$$

where $q_{I\hat{b}}$ denotes the inertial to estimated body attitude quaternion, and $\Omega(\underline{\hat{\omega}})$ is given by

$$\Omega(\underline{\hat{\omega}}) = \begin{bmatrix} -[\underline{\hat{\omega}}\times] & \underline{\hat{\omega}} \\ -\underline{\hat{\omega}}^T & 0 \end{bmatrix} \tag{2}$$

The 3x3 matrix $[\underline{\hat{\omega}}\times]$ is referred to as a cross product matrix since, for 3x1 vectors $\underline{a}$ and $\underline{b}$, $\underline{a}\times\underline{b} = [\underline{a}\times]\underline{b}$, so

$$[\underline{\hat{\omega}}\times] = \begin{bmatrix} 0 & -\hat{\omega}_3 & \hat{\omega}_2 \\ \hat{\omega}_3 & 0 & -\hat{\omega}_1 \\ -\hat{\omega}_2 & \hat{\omega}_1 & 0 \end{bmatrix} \tag{3}$$

The error quaternion is defined as

$$\delta q_{\hat{b}b} = q_{I\hat{b}}^{*} \otimes q_{Ib} \tag{4}$$

where the * denotes a quaternion inverse and $\otimes$ represents quaternion multiplication as defined in Wertz.[8]

The system equation, in state space form, is $\dot{\underline{x}} = \mathbf{F}\underline{x} + \underline{w}$ where

$$\mathbf{F} = \begin{bmatrix} -[\underline{\hat{\omega}}\times] & -\mathbf{I} \\ 0 & 0 \end{bmatrix} \tag{5}$$

The discrete solution to this system of equations is described in Gelb. For TRMM, the form of the state transition matrix is

$$\Phi = \begin{bmatrix} \Phi_1 & \Phi_2 \\ 0 & \mathbf{I} \end{bmatrix} \tag{6}$$

After some algebraic manipulation, by using the series definitions of sine and cosine and ignoring higher order terms, the submatrices can be written

$$\Phi_1 = \mathbf{I} + \hat{\omega}^{-1}\{-[\underline{\hat{\omega}}\times]\}\sin\hat{\omega}T + \hat{\omega}^{-2}\{-[\underline{\hat{\omega}}\times]\}^2(1-\cos\hat{\omega}T) \tag{7}$$

$$\Phi_2 = -\left[\mathbf{I}T + \hat{\omega}^{-2}\{-[\underline{\hat{\omega}}\times]\}(1-\cos\hat{\omega}T) + \hat{\omega}^{-3}\{-[\underline{\hat{\omega}}\times]\}^2(\hat{\omega}T-\sin\hat{\omega}T)\right] \tag{8}$$

where $\hat{\omega} \equiv |\underline{\hat{\omega}}|$.

The state noise vector, $\underline{w}$, is a zero mean, normally distributed random vector, where the state noise covariance matrix is:

$$\mathbf{Q} = \begin{bmatrix} T\sigma_v^2\mathbf{I} + \frac{T^3}{3}\sigma_u^2\mathbf{I} & -\frac{T^2}{2}\sigma_u^2\mathbf{I} \\ -\frac{T^2}{2}\sigma_u^2\mathbf{I} & T\sigma_u^2\mathbf{I} \end{bmatrix} \tag{9}$$

where σ_u is the standard deviation of gyro rate random walk and σ_v is the standard deviations of the gyro rate white noise, as used in Farrenkopf's gyro noise model. The numerical values of these variables are set based on IRU test data.

Measurement Model

Once the system equations are solved, the measurement matrix, **H**, and the measurement noise covariance matrix, **R**, must be found to complete the Kalman filter equations. The matrix **R** is empirically calculated from the noise specifications of the sensors, but the derivation of **H** is based on the geometry of the system. The measured vector, provided by either the TAM or the DSS, is $\underline{\tilde{s}}$. The expected vector, provided by the onboard ephemeris models, is $\underline{\hat{s}}$. The residual as represented in the sensor coordinate frame, $\underline{z}$, is the difference between these two vectors. The residual can be linearized as a simple subtraction by assuming only a small angle separates $\underline{\tilde{s}}$ and $\underline{\hat{s}}$:

$$\underline{z} \equiv \underline{\tilde{s}} - \underline{\hat{s}} \tag{10}$$

$$= \mathbf{A}_{bs}\mathbf{A}_{Ib}\underline{s}_I + \underline{N} - \mathbf{A}_{bs}\mathbf{A}_{I\hat{b}}\underline{s}_I \tag{11}$$

The body to sensor transformation matrix, $\mathbf{A}_{bs}$, is calculated from alignment data, and $\underline{N}$ represents the sensor noise. Since $\mathbf{A}_{Ib}$ is the inertial to true body attitude matrix, $\mathbf{A}_{Ib}\underline{s}_I = \underline{s}_b$, where $\underline{s}_b$ is the vector measured by the sensor, represented in body coordinates. The inertial to estimated body attitude matrix, $\mathbf{A}_{I\hat{b}}$, can be represented as follows:

$$\mathbf{A}_{I\hat{b}} = \mathbf{A}_{b\hat{b}}\mathbf{A}_{Ib} \tag{12}$$

Here, $\mathbf{A}_{b\hat{b}}$ is the Euler angle matrix corresponding to the attitude errors, $\underline{\delta\theta} = \begin{bmatrix} \delta\theta_x & \delta\theta_y & \delta\theta_z \end{bmatrix}^T$, which describe the difference between the true and the estimated body orientations. By assuming small angles, $\mathbf{A}_{b\hat{b}}$ reduces to

$$\mathbf{A}_{b\hat{b}} = \begin{bmatrix} 1 & -\delta\theta_z & \delta\theta_y \\ \delta\theta_z & 1 & -\delta\theta_x \\ -\delta\theta_y & \delta\theta_x & 1 \end{bmatrix} \tag{13}$$

When Equations (12) and (13) are substituted into Equation (11), and the attitude error cross product matrix is separated from $\mathbf{A}_{b\hat{b}}$, the residual can be written

$$\underline{z} = -\mathbf{A}_{bs}[\underline{\delta\theta}\times]\underline{s}_b + \underline{N} \tag{14}$$

Here, the rows of the body to sensor transformation matrix are the sensor basis vectors in the body frame:

$$\mathbf{A}_{bs} = \begin{bmatrix} \bar{u}_{sx} \\ \bar{u}_{sy} \\ \bar{u}_{sz} \end{bmatrix} \tag{15}$$

where $\bar{u}_{si}$ is the i^{th} sensor coordinate frame axis defined in body coordinates. When equation (15) is substituted into equation (14), the full residual is of the form:

$$\underline{z} = \begin{bmatrix} \bar{u}_{sx}\times\underline{s}_b & \\ \bar{u}_{sy}\times\underline{s}_b & \mathbf{0}_{3x3} \\ \bar{u}_{sz}\times\underline{s}_b & \\ \mathbf{0}_{3x3} & \mathbf{0}_{3x3} \end{bmatrix} \begin{bmatrix} \underline{\delta\theta} \\ \underline{\Delta b} \end{bmatrix} + \begin{bmatrix} \underline{N} \\ \underline{0}_{3x1} \end{bmatrix} \Leftrightarrow \underline{z} = \mathbf{H}\underline{x} + \underline{v} \tag{16}$$

This linear form of the measurement matrix, **H**, must be recalculated each time a new measurement, $\underline{s}_b$, becomes available. The measurement noise, $\underline{v}$, is a normally distributed random vector with zero mean and covariance **R**.

Algorithm Implementation

The algorithm as implemented in the TRMM flight software does not use these vector/matrix equations. Scalar processing of each measurement component is used to reduce the computational burden.[4] The TRMM implementation also includes checks on the data in the filter. The first check is made on the availability and quality of the sensor data. For example, if the sun is in the DSS field of view but the measurement is not valid, the filter will not use that DSS measurement to update the state vector. In addition, there is a residual tolerance test that rejects any measurements that yield residuals larger than a set tolerance. These checks prevent the estimation from using bad sensor data, but, since this does not constitute an algorithm failure, no corrective action is taken.

There are also three Failure Detection and Correction (FDC) checks designed specifically to monitor the Kalman filter algorithm. Two checks monitor the covariance matrix for divergence and positive semidefiniteness. The third test ensures that the residual remains within 3σ of the expected value of the residual. For all three tests, the ACS software autonomously performs the same actions. First, the software stops updating the attitude quaternion and the gyro drift with

the flawed estimation; then, it commands the spacecraft to a power and thermal safe attitude.

Algorithm Testing

The major limitation in implementing the TRMM Kalman filter was adding it to flight software already in its fourth testing cycle. Fortunately, the TRMM software was designed to allow easy replacement of individual subroutines and to provide spare space in telemetry, which facilitated adding the Kalman filter data.[9] Without this flexible software design, the addition of a software backup would have greatly impacted the schedule and software testing. In general, the tests were run to verify the nominal performance of the Kalman filter, and to ensure that the original control modes were not affected by the addition of the new algorithm.

All test results were nominal, except one. In that test, the DSS residuals failed the expected residual tolerance test after eclipse, causing the filter to reject the DSS data. This indicates that either the DSS tolerance was set too tight or that the covariance did not grow large enough during eclipse, leaving the filter knowledge of the estimation error smaller than it should have been. At the time, the ACS team believed the failure was the result of a mismatch between the 'true' ephemeris and the 'modeled' ephemeris in the test setup.

Flight Results

Sun Acquisition Mode Test

On the second day of the mission, TRMM was still in Sun Acquisition Mode holding the spacecraft inertially fixed in a power and thermal safe attitude with the +x-axis 16.5° from the sunline. In this mode, the spacecraft is controlled directly off the CSSs and the IRUs; the Kalman filter output is not used in the control loop, which provides an ideal testing situation. The Kalman filter was run for a total of 13000 seconds. After converging for 9640 seconds, the filter was reinitialized during eclipse to study the TAM- only filter performance. The TAM residuals for the entire test are shown in Figure 1. The flat line portions in this figure are periods of loss of signal (LOS), when TRMM was not in contact with the ground. It is obvious that the TAM residuals are not the zero mean, white noise processes modeled by the filter equations. The magnitude of this modeling error has implications for setting the proper sensor noise parameters in the filter that will be discussed later.

The standard deviations of the attitude estimate, shown in Figure 2, converged to [0.02°, 0.006°, 0.002°] within 8000 seconds, reaching steady state before reinitialization. The impact of the reset can be clearly seen, and the attitude estimate was still reconverging when the test ended. In Sun Acquisition Mode, the sun

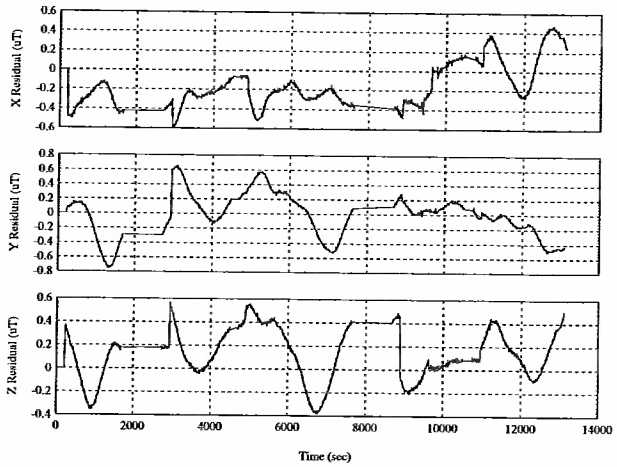

Figure 1: Sun Acquisition Mode Test: TAM Residuals

is held in the same location in the body frame, perpendicular to the z axis and primarily along the x axis. This reduces observability in the x axis, a phenomenon that is reflected in the relatives size of the attitude standard deviations, where the least observable axis corresponds to the largest steady-state value.

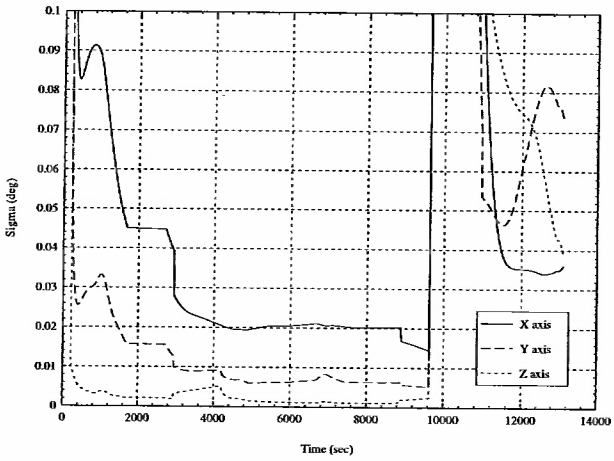

Figure 2: Sun Acquisition Mode Test: Standard Deviation of the Attitude Estimate

The DSS#1 residuals are shown in Figure 3. In the Sun Acquisition orientation only the +x DSS, DSS#1, receives sunlight, so there is no DSS#2 information available. When the Kalman filter is first enabled during sunlight, the DSS residuals were well within acceptable limits. TRMM entered sunlight about 300 seconds after the filter was reinitialized, and the DSS residual failed the 3σ tolerance check (~0.15°) after less than 700 seconds in daylight. The residual continued to fail its expected tolerance check for the entire daylight

portion of the orbit. TRMM went into eclipse before the DSS measurement was accepted again, and the test was ended.

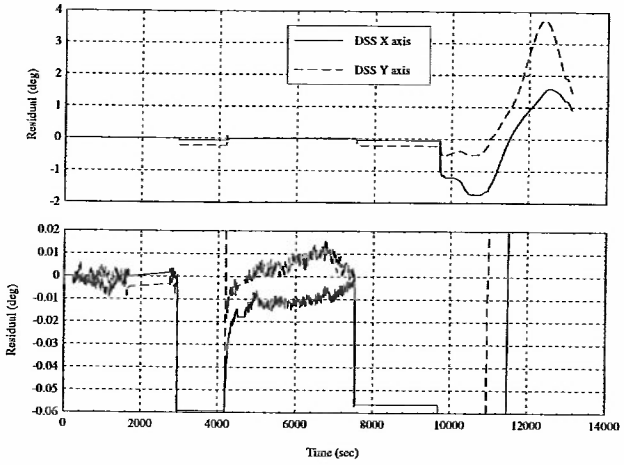

Figure 3: Sun Acquisition Mode Test: DSS#1 Residuals

This residual test failed because the actual DSS residual was larger than the expected value that is calculated from the 3σ tolerance, the state covariance, and the sensor noise. Review of the data showed that the state covariance was too small and that the 3σ tolerance was too tight. The state covariance was too small because the Kalman filter was overweighing the TAM measurement and converging too quickly. This weighting factor is a function of the TAM measurement noise covariance matrix that was set to model sensor noise on a zero mean process. As seen in Figure 1, the actual TAM measurement residual has a nonzero mean due to modeling errors. The 3σ tolerance was set too tight because the filter should be allowed to accept 5σ DSS data since the DSS was performing better than expected.

Other problems were identified later, after GSFC's Flight Dynamics Facility (FDF) had time to analyze several days of flight data. It was found that the DSS heads were misaligned by as much as 0.3°, which caused biased DSS residuals, which lead to biased estimates. Also, the influence of the MTBs on the TAM measurements had not been accurately compensated for, and that increased the bias of the TAM residuals. In addition, the IRU calibration maneuvers had not yet been completed, and the alignment matrices on-board did not properly account for the true IRU alignments. Finally, it was found that the magnetic field model on board was not internally consistent. The coefficients were from a 1995 model, but the epoch time for computation of the secular variations was set to 1990. This means that the residuals between the magnetic field model and the TAM measurements had a much larger bias and variance than expected.

Mission Mode Test

Before the next Kalman filter test, the filter parameters were retuned by modifying the on-board software tables. First, the TAM measurement noise covariance was increased from 0.25 μT^2 to 1.0 μT^2 to try to account for the model errors. Second, the DSS adjusted residual tolerance was increased from 3σ to 5σ. Third, the magnetic field model coefficients were set to the 1990 values to match the epoch time. Fourth, the DSS parameters were updated to compensate for some of the misalignment errors. The on-board software precluded compensating for the DSS misalignments completely, so there were still unmodeled DSS misalignments of up to 0.08°. Once the changes were made, the Mission Mode test began.

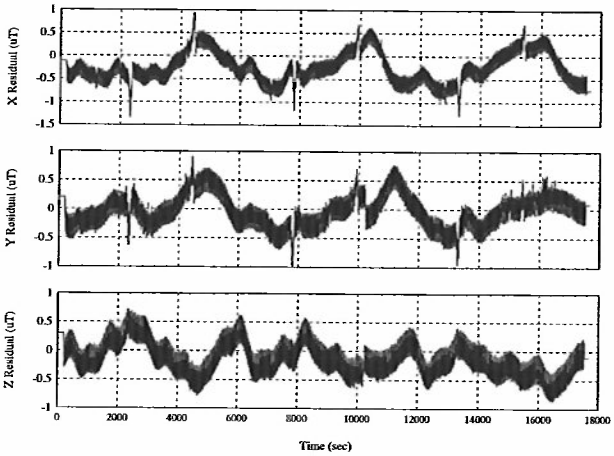

Figure 4: Mission Mode Test: TAM Residuals

The TAM residuals are shown in Figure 4, and, as in the Sun Acquisition Mode test, they are neither zero mean nor Gaussian distributed. The high frequency component of the signal is due to the unmodeled 0.5 Hz rotation of one of the payload instruments, and the low frequency variation may be due to the effects of the MTBs on the TAM measurements. The sharp spikes on the plot are caused by the sudden changes in the on-board magnetic field as the solar array current rises and falls at dawn and dusk.

The standard deviation of the attitude estimate is shown in Figure 5. The x/z (roll/yaw) quarter-orbit coupling is due to the one revolution per orbit rotation of the spacecraft about the y (pitch) axis. The spacecraft y axis is generally perpendicular to the sunline, maximizing the DSS observability, and thus shows the greatest estimated accuracy. During eclipse, the covariance increases because the less accurate TAM is the update sensor available.

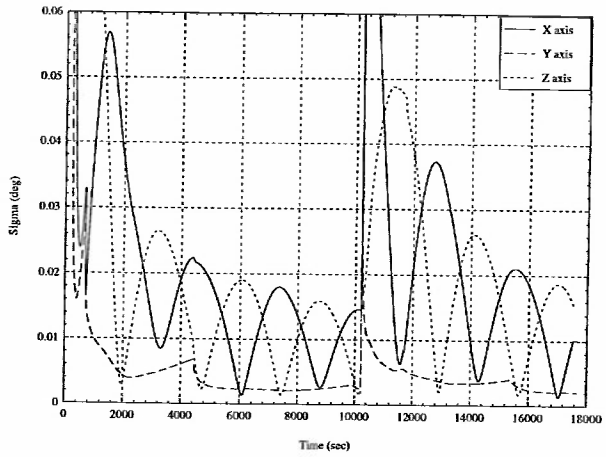

Figure 5: Mission Mode Test: Standard Deviation of the Attitude Estimate

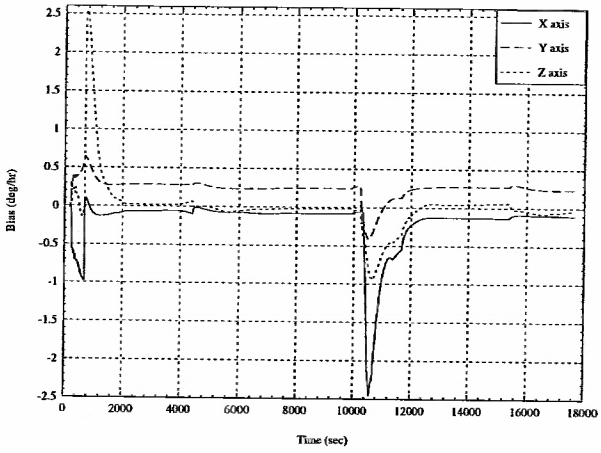

Figure 6: Mission Mode Test: Estimated Biases

Figure 6 shows that the filter estimate of the gyro biases settles to the same values before and after the reinitialization. This shows that the gyro drift is steady on a time scale of hours. This is because of the high quality and drift stability of the TRMM IRUs.

The DSS residuals are plotted in Figures 7 and 8. Between measurements, the filter simply stores the last value of the residual, and the data goes static. DSS#1 is oriented towards the +x-axis, DSS#2 is oriented towards the -x-axis, and the x axis is coincident with the orbital velocity vector during mission mode. First, one DSS detects the sun. Then, depending on the position of the sun, there may be a loss of data around orbit noon. Finally, the second DSS detects the sun. The effect of the uncompensated DSS misalignments can be seen in the large initial values of the residuals when the sun first enters the DSS field of view.

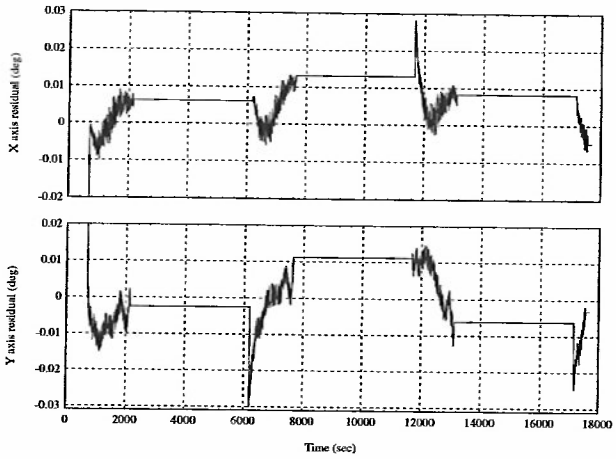

Figure 7: Mission Mode Test: DSS#1 Residuals

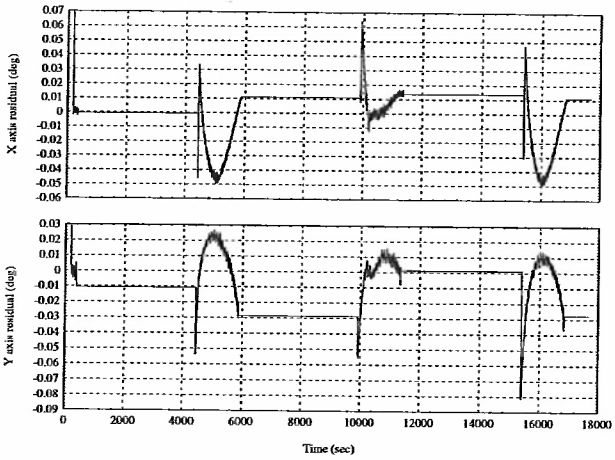

Figure 8: Mission Mode Test: DSS#2 Residuals

The best independent measure of the Kalman filter performance is the attitude derived from the ESA. Although the ESA data is not processed on board when the Kalman filter is running, the unprocessed data is available in telemetry. With this information, the ESA attitude was calculated on the ground by the ACS team, and is shown in Figure 9. The initial attitude transients are on the order of 1° in roll, and 0.2° in pitch. The best performance of the filter is the period from 5000 to 10000 seconds, when the largest attitude error is about 0.12°. During this time, an independent ground solution by FDF showed the attitude errors settling to less than 0.20°, per axis. Both the ESA and the FDF solutions verify that the steady state attitude errors are well within the 0.7° (3σ) knowledge per axis. This accuracy is due in large part to TRMM's high precision, extremely stable IRU. These results would be difficult to achieve with a less accurate gyro. The TRMM Kalman filter is the first onboard attitude estimation

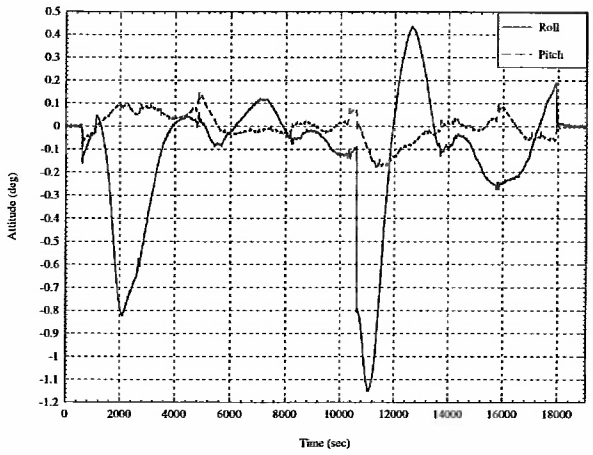

Figure 9: Mission Mode Test: ESA Attitude

algorithm at GSFC to use a DSS and a TAM to estimate attitude better than 0.25°.

Lessons Learned

The possible improvements in the TRMM Kalman filter fall into three basic categories: operational issues, performance issues, and implementation features. Operational issues include transitions to the backup mode, testing, software design, and data flow. Performance issues pertain to properly tuning a Kalman filter so that it functions effectively with real sensors. Implementation features concerns algorithm and software design.

Operations issues

Since the TRMM Kalman filter was added late in the testing cycle, the concern about onboard processing power forced the software design to an either/or mindset. Either the ESA processing or the Kalman filter could be run, but not both. Assuming the filter only had to replace the ESA functions meant that the filter's performance during other cases, such as thruster maneuvers, was not thoroughly considered. This led to several logistical oversights in the filter design. The software propagates the attitude estimate during thruster maneuvers, but it does not propagate the filter covariance. Thus, after completing the thruster burn, the covariance gives an incorrect indication of the accuracy of the attitude estimate. To remedy this situation, the filter must be reinitialized after each thruster burn. However, the reconvergence reduces the quality of the science data for several hours.

Also, since the filter was designed to replace a failed ESA, it was assumed that once the Kalman filter was turned on, it would never be turned off. So, the ground verification did not test the transition between the filter and ESA processing. Again, this led to several oversights. First, the filter continually estimates the gyro biases. When the filter stops running, these bias estimates are frozen in memory. As the spacecraft's orientation changes, misalignment errors map differently into the gyro drift bias errors. If the filter is running, these changes will be compensated for on board. If the filter is not running, the estimate that is in memory may actually introduce a small error in the drift biases. Thus, it is necessary to reset the gyro drift biases after exiting the filter. To zero the estimated bias, the gyro initialization subroutine must be rerun. In the initial software design, this could only be accomplished by rebooting the ACS software, which is extremely risky during flight. To eliminate this risk, a separate gyro reset command had to be incorporated into the ACS software a few months prior to launch. Including the zeroing of this initial biases in the original filter initialization subroutine would have been a much cleaner solution.

These issues make the transition between ESA attitude determination and Kalman filter attitude determination unnecessarily awkward, and complicated the on-orbit testing. The initial assumptions concerning the use of the Kalman filter limited the design and the filter operation.

Performance issues

The Kalman filter models assume zero-mean white noise measurement residuals, which is mostly true of the DSS residuals but is not true of the TAM residuals. Also, the filter has no knowledge of biased sensor readings unless they are included in the state equations, so the DSS misalignment has a large impact on the accuracy of the filter. To better characterize the estimation errors, the sensors and relevant instruments must be accurately modeled in the simulation including biases, scale factor errors, and misalignments. In particular, an accurate gyro model is essential if gyro biases are included in the filter states. Also, the full effects of the Earth's magnetic field on the Kalman filter cannot be properly seen in simulation because the low frequency variations of the Earth's magnetic field are hard to model accurately. Ideally, the simulation should model all of the errors that will be seen on orbit, but that is not always easy to achieve.

As mentioned previously, FDC is designed to capture certain problems, and to keep the spacecraft safe. The three FDC tests discussed will not indicate if the filter is trying to estimate an attitude error or a gyro bias error larger than it was told to expect. If the true error is larger than the error indicated by state covariance, the filter may converge to an incorrect attitude. This type of error is indicated when the filter's estimates do not match the true attitude. Outside of a computer simulation, however, there is no truth model to use for comparison. If this type of problem is suspected, the best option is to compare the estimates from the filter

to ground estimates and adjust, or tune, the filter based on the comparison, a luxury that is not always available to the operations team. To properly tune a filter, the designers must be aware of the largest possible state error, and choose initial state covariance values larger than the expected error. Even though this greatly increases the filter's convergence time, it will allow the filter to converge from larger, more uncertain initial estimation errors. This is obviously a filter design tradeoff.

Implementation features

The flight software developers should avoid hardcoding values; a table-based design allows parameters to be changed with a simple uplink. Software patches require significant development and testing, and risk the safety of the spacecraft. For example, some of the DSS misalignment error was calibrated out of the data by modifying table values, but updating the magnetic field model to a 1995 epoch will require a software change.

There should be a control mode available to check out the Kalman filter performance before controlling with the filter's attitude estimates. On TRMM, the Sun Acquisition control mode uses the CSSs and IRUs for attitude determination, which allowed the filter to be tested in-flight without affecting the safety of the spacecraft. If the processing power had been sufficient to run both the Kalman filter and the ESA processing, much of the awkward testing done on TRMM would have been unnecessary. Running both algorithms simultaneously would provide two attitude estimates at all times, allowing ground personnel the luxury of evaluating the long term performance of the filter without affecting nominal mission operations.

The FDC logic is a vital safety feature of the TRMM design. With these tests, the on-board algorithm determines when it is inappropriate to use the filter results. If a bad attitude estimate is computed, the software stops updating the filter states and autonomously places the spacecraft in a power and thermal safe orientation.

Decisions to incorporate backups for hardware failures, whether using redundant hardware or implementing software backups, should be made early in the program, so that the additional processing needs would be reflected in the processor requirements and design. Once backups algorithms are selected, good subsystem engineering should help identify all possible uses of these algorithms so those conditions can be tested. As the discussion of the thruster maneuvers reveals, 'expected' usage tests do not cover all reasonable situations. This experience shows that software designed for one spacecraft can be reused on a different spacecraft if the software design is modular enough and the reused software is well tested. The fundamental lesson learned is that adding redundancy using "just software" underestimates the difficulty of doing the job properly.

Conclusion

In the unlikely event of a complete ESA failure, TRMM can meet pointing requirements by using TAM and DSS data. The additional software in the form of an extended Kalman filter saved the expense of buying backup attitude sensors. It was not easy to convert existing software, but the software modifications were completed quickly, largely due to the modular design of the RXTE and TRMM software. Pre-flight testing of the software was extensive, but it did not identify all the problems encountered on orbit, both because there was not enough time to modify the simulation system to include all known error sources, and because some unexpected errors showed up in flight tests. However, flight testing showed excellent estimation performance largely due to the high accuracy IRUs. Pointing performance was better than the required 0.7°, and approached the 0.2° performance of the primary attitude determination system.

References

[1]D. Ward, internal memo, "TRMM ACS Peer Review Action Items Regarding Earth Sensor Assembly Concerns", August 18, 1992.

[2]J.L. Crassidis, S.F. Andrews, F.L. Markley, K. Ha, "Contingency Designs for Attitude Determination of TRMM", Flight Mechanics/Estimation Theory Symposium, 1995.

[3]Hashmall, J.A., Rokni, M., Sedlak, J., Harman, R., Ketchum, E., *How Accurate an Attitude Can We Get Using Magnetometers?*, Flight Mechanics/Estimation Theory Symposium, 1994.

[4]Murrell, J.W., "Precision Attitude Determination for Multimission Spacecraft," AIAA Paper 78-1248, Aug. 1978.

[5]Lefferts, E.J., Markley, F.L., and Shuster, M.D., "Kalman Filtering for Spacecraft Attitude Estimation," *Journal of Guidance, Navigation, and Control*, Sept.-Oct. 1982.

[6]Gelb, A. (ed.), *Applied Optimal Estimation*, The MIT Press, Cambridge, MA, 1974.

[7]Farrenkopf, R.L., "Analytical Steady-State Accuracy Solution for Two Common Spacecraft Attitude Estimators," *Journal of Guidance and Control*, Vol. 1, No. 4, July-Aug, 1978. pp.282-284.

[8]Wertz, J.S. (ed.), *Spacecraft Attitude Determination and Control*, D. Reidel Publishing Co., Dordrecht, The Netherlands, 1984.

[9]Andrews, S.F., D'Agostino, J.M., "Development, Implementation, and Testing of the TRMM Kalman Filter," Flight Mechanics Symposium, 1997.